QCD analysis of polarized DIS and the SIDIS asymmetry world data and light sea-quark decomposition

F. Arbabifar,[*] Ali N. Khorramian,[†] and M. Soleymaninia[‡]

Faculty of Physics, Semnan University, Semnan, Iran and School of Particles and Accelerators, Institute for Research in Fundamental Sciences (IPM), P.O. Box 19395-5531, Tehran, Iran

(Received 11 November 2013; published 7 February 2014)

The results of our new QCD analysis of helicity parton distributions of the nucleon at full next-to-leading order accuracy in the fixed-flavor number scheme are presented. Performing a combined QCD fit on the global sets of latest inclusive and the semi-inclusive polarized deep inelastic scattering data, we are able to extract new polarized parton distribution functions (PPDFs) at the input scale $Q_0^2 = 1$ GeV^2. Particularly, we calculate PPDFs considering light sea-quark decomposition, and the results are compared with the experimental data and the most precise theoretical models obtained by recent analyses. The latest COMPASS2010 SIDIS data, which were not used in the combined analyses before 2010, are employed in the current analysis, and the effect of COMPASS SIDIS data is studied in detail. Also, the uncertainties of PPDFs are determined using the standard Hessian technique.

DOI: 10.1103/PhysRevD.89.034006 PACS numbers: 13.60.Hb, 12.39.-x, 14.65.Bt

I. INTRODUCTION

In recent years, the determination of nucleon partonic composition and their spin projections from high energy experimental data has improved remarkably, and the extracted polarized and unpolarized partonic distributions have a very essential role in the study of hard scattering processes phenomenology. For the case of polarized parton distributions, the experimental discoveries of nucleon spin in the late 1980s [1,2] proved that the spin contribution of valence quarks is anomalously small. They also showed that the predictions are far from the reality, and then the theoretical assumptions on perturbative QCD were applied to interpret theses experimental results [3–7].

In recent decades, the determination of polarized parton distribution functions (PPDFs) and their uncertainties from deep inelastic scattering (DIS) experiments performed at CERN, SLAC, DESY, and JLAB [1,2,8–19] spread very fast [20–45], and recently semi-inclusive deep inelastic scattering (SIDIS) experimental data [15,46–48] have also been included by some of the theoretical groups [49–53]. The only theoretical group which performed a combined NLO analysis of DIS, SIDIS, and polarized proton-proton collision data was DSSV in 2008 [54]. The extracted PPDFs of valence quarks lightly differ, but the PPDFs of sea quarks and gluons have larger differences caused by data set selection, parametrization forms of PPDFs, and the methods of evolution and QCD analysis. The effects of different PPDFs and the spin physics on the determination of fragmentation functions (FFs) have been studied recently in Ref. [55].

In our latest analysis, we studied the impact of inclusive DIS data on the determination of PPDFs based on Jacobi polynomials with flavor symmetric light sea distribution, i.e., $\delta\bar{u} = \delta\bar{d} = \delta\bar{s} = \delta s$ [21], and now we consider light sea-quark decomposition and include additional SIDIS data [15,46–48,56]. In fact, fully inclusive DIS data from many different experiments are just as impressive at determining the sum of the quark and antiquark distributions, while SIDIS data help to tell the difference between quarks and antiquarks as well. Here we focus on the effect of SIDIS data on the determination of PPDFs, especially the sea quarks' distribution separation which was not considered in our last DIS data analysis, and we present a comparison of both results. The impact of RHIC polarized proton-proton collision data will be studied in a separate publication in the near future.

In the present analysis, we utilize the full sets of proton and deuteron SIDIS asymmetry data from the COMPASS group at CERN [47,48,56] which were partially considered by the last analysis on SIDIS data [49,54]. In particular, we use the new semi-inclusive asymmetries' COMPASS2010 proton data for charged pion and kaon production from a polarized proton target, $A_1^{p,\pi^{\pm}}$ and $A_1^{p,k^{\pm}}$ [56]. These data were not available for the analysis before 2010, and they are helpful to study δs and $\delta\bar{s}$ distributions due to kaon detection from polarized protons for the first time [56]. In order to discuss more about the effect of COMPASS SIDIS data on polarized $\bar{u}$, $\bar{d}$, and $s = \bar{s}$, we perform an extra analysis excluding these data sets. The comparison of results shows the effect of their inclusion clearly.

The current study presents a new next-to-leading order (NLO) QCD analysis of the polarized DIS and SIDIS data, and we extract new parametrization forms of PPDFs in

[*]farbabifar@ipm.ir
[†]khorramiana@theory.ipm.ac.ir
[‡]maryam_soleymaninia@ipm.ir

flavor SU(2) and SU(3) symmetry breaking. Here we also propose a simplified form of double Mellin convolution expressions which saves time during the fitting procedure. Also, the behavior of $\Delta\chi^2$ and the uncertainty of PPDFs are calculated using the standard Hessian method.

This paper is organized as follows. In Sec. II we present the relationship between polarized structure functions and asymmetry data as observables, and then we review the data sets used in our analysis on PPDFs. QCD analysis including parametrization, evolution, and the simplification of double Mellin convolution are discussed in Sec. III. Section V presents the fitting procedure and global χ^2 minimization for asymmetry data and the investigation of the χ^2 neighborhood and error calculation by the standard Hessian method. We present the full results of our fit to the data, comparison with other models, and sum rules in Sec. VI, and finally Sec. VII contains the summary of the whole work.

II. EXPERIMENTAL OBSERVABLES AND DATA SETS

A. Polarized asymmetries

Perturbative QCD can predict the polarized structure function $g_1(x,Q^2)$ in terms of PPDFs and the strong coupling constant up to a NLO approximation. However, experimental groups measure cross section asymmetries $A_\parallel$ and $A_\perp$, defined by the following ratios:

$$A_\parallel = \frac{d\sigma^{\rightarrow\Rightarrow} - d\sigma^{\rightarrow\Leftarrow}}{d\sigma^{\rightarrow\Rightarrow} + d\sigma^{\rightarrow\Leftarrow}}, \qquad A_\perp = \frac{d\sigma^{\rightarrow\Uparrow} - d\sigma^{\rightarrow\Downarrow}}{d\sigma^{\rightarrow\Uparrow} + d\sigma^{\rightarrow\Downarrow}}, \quad (1)$$

where $d\sigma^{\rightarrow\Rightarrow}$ and $d\sigma^{\rightarrow\Leftarrow}$ are cross sections for longitudinal polarized lepton scattering of a parallel or antiparallel polarized target hadron, and $d\sigma^{\rightarrow\Uparrow}$ and $d\sigma^{\rightarrow\Downarrow}$ are the same for a transversely polarized hadron.

The ratio of polarized and unpolarized structure functions, g_1 and F_1, is related to the measurable asymmetries by

$$\frac{g_1(x,Q^2)}{F_1(x,Q^2)} = \frac{1}{(1+\gamma^2)(1+\eta\zeta)}\left[(1+\gamma\zeta)\frac{A_\parallel}{D} - (\eta-\gamma)\frac{A_\perp}{d}\right], \quad (2)$$

and the definitions of kinematic factors are given by

$$\gamma = \frac{2Mx}{\sqrt{Q^2}}, \quad (3)$$

$$d = \frac{D\sqrt{1-y-\gamma^2y^2/4}}{1-y/2}, \quad (4)$$

$$D = \frac{1-(1-y)\epsilon}{1+\epsilon R(x,Q^2)}, \quad (5)$$

$$\eta = \frac{\epsilon\gamma y}{1-\epsilon(1-y)}, \quad (6)$$

$$\zeta = \frac{\gamma(1-y/2)}{1+\gamma^2 y/2}, \quad (7)$$

$$\epsilon = \frac{4(1-y)-\gamma^2y^2}{2y^2+4(1-y)+\gamma^2y^2}, \quad (8)$$

where M denotes the nucleon mass and $y = (E-E')/E$ describes the normalized energy fraction transferred to the virtual photon, with E the energy of the incoming lepton and E' the energy of the scattered lepton in the nucleon rest frame. The unpolarized structure function F_1 is expressed by its expression in terms of measured unpolarized structure function F_2 extracted from unpolarized DIS experiments [57],

$$F_1(x,Q^2) = \frac{(1+\gamma^2)}{2x(1+R(x,Q^2))}F_2(x,Q^2), \quad (9)$$

and R is the ratio of the longitudinal to transverse photon-nucleon unpolarized structure function, which is determined in Ref. [58]:

$$R(x,Q^2) = \frac{F_L(x,Q^2)}{F_2(x,Q^2)-F_L(x,Q^2)}. \quad (10)$$

The asymmetries $A_\parallel$ and $A_\perp$ can be expressed in terms of A_1 and A_2, which are the virtual-photon longitudinal and transverse asymmetries, by

$$A_\parallel = D(A_1+\eta A_2), \qquad A_\perp = d(A_2-\zeta A_1), \quad (11)$$

where

$$A_1(x,Q^2) = \frac{\sigma^T_{1/2}-\sigma^T_{3/2}}{\sigma^T_{1/2}+\sigma^T_{3/2}}, \qquad A_2(x,Q^2) = \frac{2\sigma^{TL}}{\sigma^T_{1/2}+\sigma^T_{3/2}}. \quad (12)$$

Note that $\sigma^T_{1/2}$ and $\sigma^T_{3/2}$ recall the virtual transversely polarized photon scattering cross sections when the total spin of the photon-nucleon system is $1/2$ or $3/2$, respectively, and σ^{TL} is the term denoting the interference of longitudinal and transverse photon-nucleon amplitudes. Finally, using Eqs. (11) and (2) one can find the relation between polarized and unpolarized structure functions g_1 and F_1, and the asymmetries A_1 and A_2 [59]:

$$\frac{g_1}{F_1} = \frac{1}{1+\gamma^2}[A_1+\gamma A_2]. \quad (13)$$

The value of A_2 has been determined by SMC [60], E154 [61], and E143 [62], and the measurements showed that its

contribution to g_1/F_1 can be neglected in a good approximation. Also, it is being suppressed by the small value of the kinematic factor γ in the limit $m^2 \ll Q^2$.

In our QCD analysis, we perform a fit procedure on A_1 or g_1/F_1 for DIS data:

$$A_1(x,Q^2) = \frac{g_1(x,Q^2)}{F_1(x,Q^2)}(1+\gamma^2). \tag{14}$$

Note that such a procedure is equivalent to a fit to $(g_1)_{\rm exp}$, but it is more precise than the fit to the g_1 data themselves presented by the experimental groups, because here the g_1 data are extracted in the same way for all of the data sets.

Unlike the inclusive polarized deep inelastic scattering wherein the g_1 structure function is measured by detecting only the final state lepton, the particles detected in semi-inclusive polarized deep inelastic experiments are charged hadrons in addition to scattered leptons. When the energy fraction of a hadron, $z = E_h/E_\gamma$, is large, the most possible occurrences of detected hadrons are $\pi^\pm$ and $k^\pm$, which include struck quarks in their valance state. The double-spin asymmetry in SIDIS experiments for the production of hadron h is

$$A_{1N}^h(x,z,Q^2) = \frac{g_{1N}^h(x,z,Q^2)}{F_{1N}^h(x,z,Q^2)}. \tag{15}$$

The structure functions g_1^h and F_1^h are fully determined in terms of polarized and unpolarized distributions, respectively, up to the NLO approximation, and they will be discussed in Sec. III. Thus, we will determine g_1 and g_{1N}^h from Eqs. (14) and (15) in the analysis and extract polarized parton distribution functions.

B. The data sets and ranges

We utilize two types of data sets from DIS and SIDIS experiments which come from relevant experiments done at DESY, SLAC, JLAB, and CERN. The data sets used in our QCD analysis are summarized in Table I. These experiments have different targets, including protons, neutrons, and deuterons, and also different detected hadrons, including $\pi^\pm$, $k^\pm$, and $h^\pm$, for SIDIS reactions. We also show the number of data and the kinematic cuts on the experiments in Table I; we exclude the data points which are in the range of $Q^2 < 1$ from our analysis since below $Q^2 = 1$ GeV^2, perturbative QCD is not reliable. The summary of observables is as follows:

(i) *EMCp, SMCpd, COMPASS, E142, E143, E154, E155 HERMES, and JLAB DIS data*
These experiments all determined A_1 except for E155 [13,14] and HERMES [16] which present g_1/F_1 and JLAB [18] which presents both measurements. Since we consider different masses of nucleons in γ in Eq. (14), we distinguish these two data types.

(ii) *SMCpd, HERMES, and COMPASS SIDIS data*
These experiments measure A_{1N}^h as in Eq. (15) from semi-inclusive reactions. The very recent and precise proton data of COMPASS [56], which were not available for the analysis before 2010, are used in the current analysis. Figures 1 and 2 show the data points used for DIS and SIDIS in a scatter plot; as can be seen, the regions of x and Q^2 are restricted to $0.004 \lesssim x \lesssim 0.75$ and $1.0 \lesssim Q^2 \lesssim 60$ GeV^2 for DIS and $0.005 \lesssim x \lesssim 0.5$ and $1.0 \lesssim Q^2 \lesssim 60$ GeV^2 for SIDIS experiments. We try to use all available data for DIS and SIDIS experiments to cover a large range of kinematics variables in comparison to other recent analyses [23,49,54].

III. DETERMINATION OF POLARIZED PDFS FROM OBSERVABLES

A. Theoretical framework

The main idea behind our present analysis is to extract the universal polarized PDFs entering factorized cross sections. This procedure is done by optimizing the agreement between the measured asymmetries from DIS and SIDIS experiments through the variation of the shapes of the polarized PDFs. It is also relative to the accuracy of the data and corresponding theoretical calculations.

Considering perturbative QCD, the structure function $g_1(x,Q^2)$ can be written in NLO approximation as a Mellin convolution of the PPDFs, including gluons, with the corresponding Wilson coefficient functions $\delta C_{q,g}$ [6], as

$$g_1(x,Q^2) = \frac{1}{2}\sum_{q,\bar q}^{n_f} e_q^2 \left\{ \left[1 + \frac{\alpha_s}{2\pi}\delta C_q\right] \otimes \delta q(x,Q^2) + \frac{\alpha_s}{2\pi} 2\delta C_g \otimes \delta g(x,Q^2)\right\}, \tag{16}$$

where e_q denotes the charge of the quark flavor and $\{\delta q, \delta\bar q, \delta g\}$ are the polarized quark, antiquark, and gluon distributions, respectively.

For the SIDIS asymmetry of Eq. (15), we have the following forms for polarized and unpolarized structure functions in NLO approximation:

$$g_{1N}^h(x,z,Q^2) = \frac{1}{2}\sum_{q,\bar q}^{n_f} e_q^2 \left\{ \left[\delta q \left(1 + \otimes \frac{\alpha_s(Q^2)}{2\pi}\delta C_{qq} \otimes\right) D_q^h + \delta q \otimes \frac{\alpha_s(Q^2)}{2\pi}\delta C_{gq}^{(1)} \otimes D_g^h + \delta g \otimes \frac{\alpha_s(Q^2)}{2\pi}\delta C_{qg}^{(1)} \otimes D_q^h\right](x,z,Q^2)\right\}, \tag{17}$$

and

TABLE I. Published data points from experimental groups, the process they are extracted from, the number of them (with a cut of $Q^2 \geq 1.0$ GeV^2), their kinematic range, the measured observables, and the χ^2 values for each set.

Experiment	Process	N_{data}	x_{min}	x_{max}	Q^2_{min} [GeV^2]	Q^2_{max} [GeV^2]	F	χ^2
EMC [1,2]	DIS(p)	10	0.015	0.466	3.5	29.5	A_1^p	3.9
SMC [8]	DIS(p)	12	0.005	0.48	1.3	58	A_1^p	3.4
SMC [8]	DIS(d)	12	0.005	0.479	1.3	54.8	A_1^d	17.1
COMPASS [9]	DIS(p)	15	0.0046	0.568	1.1	62.1	A_1^p	20.5
COMPASS [9]	DIS(d)	15	0.0046	0.566	1.1	55.3	A_1^d	13.6
SLAC/E142 [10]	DIS(n)	8	0.035	0.466	1.1	5.5	A_1^n	4.18
SLAC/E143 [11]	DIS(p)	28	0.031	0.749	1.27	9.52	A_1^p	22.0
SLAC/E143 [11]	DIS(d)	28	0.031	0.749	1.27	9.52	A_1^d	54.6
SLAC/E154 [12]	DIS(n)	11	0.017	0.564	1.2	15	A_1^n	3.3
SLAC/E155 [13]	DIS(p)	24	0.015	0.75	1.22	34.72	$\frac{g_1^p}{F_1^p}$	22.5
SLAC/E155 [14]	DIS(d)	24	0.015	0.75	1.22	34.72	$\frac{g_1^d}{F_1^d}$	21.4
HERMES [15]	DIS(p)	9	0.033	0.447	1.22	9.18	A_1^p	4.5
HERMES [15]	DIS(d)	9	0.033	0.447	1.22	9.16	A_1^d	11.4
HERMES [16]	DIS(n)	9	0.033	0.464	1.22	5.25	A_1^n	2.5
HERMES [16]	DIS(p)	19	0.028	0.66	1.01	7.36	$\frac{g_1^p}{F_1^p}$	21.4
HERMES [17]	DIS(p)	15	0.0264	0.7248	1.12	12.21	A_1^p	10.2
HERMES [17]	DIS(d)	15	0.0264	0.7248	1.12	12.21	A_1^d	16.7
JLab-Hall A [18]	DIS(n)	3	0.33	0.6	2.71	4.38	$\frac{g_1^n}{F_1^n}$	0.8
CLAS [19]	DIS(p)	151	0.1088	0.5916	1.01	4.96	A_1^p	151.0
CLAS [19]	DIS(d)	482	0.1366	0.57	1.01	4.16	A_1^d	442.5
SMC [46]	SIDIS(p, h^+)	12	0.005	0.48	10	10	A_1^{p,h^+}	23.0
SMC [46]	SIDIS(p, h^-)	12	0.005	0.48	10	10	A_1^{p,h^-}	11.9
SMC [46]	SIDIS(d, h^+)	12	0.005	0.48	10	10	A_1^{d,h^+}	6.3
SMC [46]	SIDIS(d, h^-)	12	0.005	0.48	10	10	A_1^{d,h^-}	17.2
HERMES [15]	SIDIS(p, h^+)	9	0.034	0.448	1.21	9.76	A_1^{p,h^+}	15.0
HERMES [15]	SIDIS(p, h^-)	9	0.034	0.448	1.21	9.76	A_1^{p,h^-}	6.0
HERMES [15]	SIDIS(p, h^+)	9	0.033	0.446	1.21	9.61	A_1^{d,h^+}	10.3
HERMES [15]	SIDIS(d, h^-)	9	0.033	0.446	1.21	9.61	A_1^{d,h^-}	8.9
HERMES [15]	SIDIS(p, π^+)	9	0.033	0.449	1.22	10.46	A_1^{p,π^+}	9.7
HERMES [15]	SIDIS(p, π^-)	9	0.033	0.449	1.22	10.46	A_1^{p,π^-}	7.7
HERMES [15]	SIDIS(d, π^+)	9	0.033	0.446	1.22	10.24	A_1^{d,π^+}	18.2
HERMES [15]	SIDIS(d, π^-)	9	0.033	0.446	1.22	10.24	A_1^{d,π^+}	25.0
HERMES [15]	SIDIS(d, k^+)	9	0.033	0.447	1.22	10.26	A_1^{d,k^+}	10.3
HERMES [15]	SIDIS(d, k^-)	9	0.033	0.447	1.22	10.26	A_1^{d,k^-}	6.1
COMPASS [47]	SIDIS(d, h^+)	12	0.0052	0.482	1.17	60.2	$A_d^{h^+}$	18.1
COMPASS [47]	SIDIS(d, h^-)	12	0.0052	0.482	1.17	60.2	$A_d^{h^-}$	20.2
COMPASS [48]	SIDIS(d, π^+))	10	0.0052	0.24	1.16	32.8	$A_d^{\pi^+}$	13.8
COMPASS [48]	SIDIS(d, π^-)	10	0.0052	0.24	1.16	32.8	$A_d^{\pi^-}$	14.6
COMPASS [48]	SIDIS(d, k^+)	10	0.0052	0.24	1.16	32.8	$A_d^{k^+}$	24.0
COMPASS [48]	SIDIS(d, k^-)	10	0.0052	0.24	1.16	32.8	$A_d^{k^-}$	14.4
COMPASS10 [56]	SIDIS(p, π^+)	12	0.0052	0.48	1.16	55.6	$A_p^{\pi^+}$	15.7
COMPASS10 [56]	SIDIS(p, π^-)	12	0.0052	0.48	1.16	55.6	$A_p^{\pi^-}$	11.2
COMPASS10 [56]	SIDIS(p, k^+)	12	0.0052	0.48	1.16	55.6	$A_p^{k^+}$	14.3
COMPASS10 [56]	SIDIS(p, k^-)	12	0.0052	0.48	1.16	55.6	$A_p^{k^-}$	6.4
TOTAL:		1149						1171.5

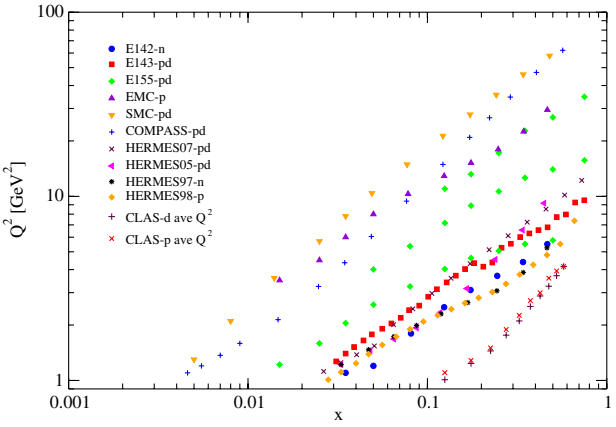

FIG. 1 (color online). Data used for DIS in an (x, Q^2) plane.

$$F_{1N}^h(x,z,Q^2) = \frac{1}{2}\sum_{q,\bar{q}}^{n_f} e_q^2 \Big\{ \Big[q\Big(1+ \otimes \frac{\alpha_s(Q^2)}{2\pi} C_{qq} \otimes\Big) D_q^h + q \otimes \frac{\alpha_s(Q^2)}{2\pi} C_{gq}^{(1)} \otimes D_g^h + g \otimes \frac{\alpha_s(Q^2)}{2\pi} C_{qg}^{(1)} \otimes D_q^h \Big](x,z,Q^2) \Big\}, \tag{18}$$

where δq and q denote polarized and unpolarized parton distributions, and $\delta C_{ij}^{(1)}(x,z)$ and $C_{ij}^{(1)}(x,z)$, $i, j = q, g$, are Wilson coefficient functions presented in Ref. [63] in the $\overline{\text{MS}}$ scheme. Also, $D_{q,\bar{q}}^h$, D_g^h denote the corresponding fragmentation functions and n_f presents the number of active flavors, which we take as $n_f = 3$ in the present analysis.

As can be seen, the SIDIS asymmetries depend on the hadronic variable $z = p_h.p_N/p_N.q$ in addition to x and Q^2. Here z denotes the momentum fractions taken by the resulting hadron from the scattered parton, and p_h, p_N, and q are the usual hadron, nucleon, and photon four-momenta, respectively. Since experimental collaborations

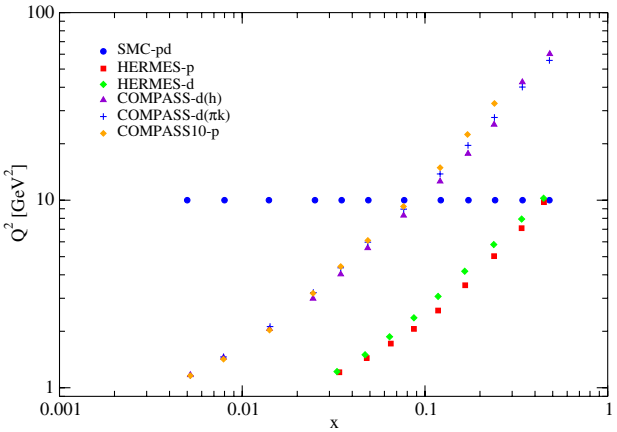

FIG. 2 (color online). Data used for SIDIS in an (x, Q^2) plane.

do not present the z variable of presented SIDIS data points, we integrate over $z > 0.2$, which comes from the current fragmentation functions region, for both $g_1(x,z,Q^2)$ and $F_1(x,z,Q^2)$ to cancel the z dependance of A_{1N}^h [64]:

$$A_{1N}^h(x,z,Q^2) = \frac{\int_{0.2}^1 dz g_{1N}^h(x,z,Q^2)}{\int_{0.2}^1 dz F_{1N}^h(x,z,Q^2)}. \tag{19}$$

One of the most important ingredient of SIDIS data analysis is the choice of fragmentation functions [65]. Although there are different available analyses of FFs [55,66,67], here we use the latest DSS [68] NLO FFs and for unpolarized PDFs we choose MRST02 [69] parametrization like DSSV09 and LSS10 [49,54] to make our analysis comparable with them. Also, in addition to the precision of the above FFs and PDFs and comparability, we use them together since DSS FFs were extracted from SIDIS data using MRST02 unpolarized PDFs.

Considering isospin symmetry, one can relate proton and neutron parton distributions,

$$\begin{aligned} &\delta u^p = \delta d^n, \quad \delta\bar{u}^p = \delta\bar{d}^n, \quad \delta d^p = \delta u^n, \\ &\delta\bar{d}^p = \delta\bar{u}^n, \quad \delta s^p = \delta s^n, \quad \delta\bar{s}^p = \delta\bar{s}^n, \end{aligned} \tag{20}$$

so the polarized structure function of neutron g_1^n can be obtained from all of Eqs. (16)–(18) by just replacing up-quark PPDFs and FFs with down ones. Also, deuteron structure functions are given in terms of proton and neutron ones in the effective polarization approximation (EPA) [70]

$$g_{1d}^{(h)} = \frac{1}{2}(g_{1p}^{(h)} + g_{1n}^{(h)})(1\text{–}1.5\omega_D), \tag{21}$$

where $(1\text{–}1.5\omega_D)$ is the average polarization of proton and neutron in the static limit and $\omega_D = 0.05$ is the probability to find the deuteron in a D state. Typically the binding energies of deuterium and ^{3}He targets are small in comparison with the momentum transfers Q^2 in the current experiments, so the effects of nuclear binding and Fermi motion are negligible in a good approximation in the present analysis. Recently the nuclear corrections have been considered in a global analysis of polarized DIS experiments in Ref. [70], and the results are compared to the analysis without the corrections.

Now by having PPDFs and all other ingredients, we are able to make polarized asymmetry functions from DIS and SIDIS processes.

B. PPDFs parametrization

In our analysis, we choose an initial scale for the evolution of $Q_0^2 = 1$ GeV^2 and assume the PPDFs to have the following functional form:

$$x\delta q = \mathcal{N}_q \eta_q x^{a_q}(1-x)^{b_q}(1 + c_q x^{0.5} + d_q x), \tag{22}$$

with $\delta q = \delta u + \delta\bar{u}$, $\delta d + \delta\bar{d}$, $\delta\bar{u}$, $\delta\bar{d}$, $\delta\bar{s}$, and δg. The normalization constants $\mathcal{N}_q$

$$\frac{1}{\mathcal{N}_q} = \left(1 + d_q \frac{a_q}{a_q + b_q + 1}\right) B(a_q, b_q + 1) + c_q B\left(a_q + \frac{1}{2}, b_q + 1\right), \quad (23)$$

are chosen such that η_q are the first moments of $\delta q(x, Q_0^2)$ and $B(a, b)$ is the Euler beta function. Since the present SIDIS data are not yet sufficient to distinguish s from $\bar{s}$, we assume $\delta s(x, Q^2) = \delta\bar{s}(x, Q^2)$ throughout.

To control the behavior of PPDFs, we have to consider some extra constraints; so we get $a_{u+\bar{u}} = a_{\bar{u}}$ and $a_{d+\bar{d}} = a_{\bar{d}} = a_s$ to control the small x behavior of $\bar{u}$, $\bar{d}$, and $s = \bar{s}$. Also, in the primary fitting procedures we find out that the parameters $b_{\bar{u}}$, $b_{\bar{d}}$, $b_{s=\bar{s}}$, and b_g become very close to one another, around 10. We understand that they are not strongly determined by the fit, so we fix them at 10, which is their preferred value to fulfill the positivity condition, $|\delta q_i(x, Q_o^2)| \leq q_i(x, Q_0^2)$ [71], and also it controls the behavior of polarized sea quarks at large x region. In addition, we find that the parameter c_q is very close to zero for $\delta q = \delta u + \delta\bar{u}$, $\delta d + \delta\bar{d}$, $\delta\bar{s}$, and δg, so we fix them at 0.

Generally, PPDFs analyses use two well-known sum rules relating the first moments of PPDFs to F and D quantities which are evaluated in neutron and hyperon β decays [72] under the assumption of SU(2) and SU(3) flavor symmetries,

$$a_3 = \Delta\Sigma_u - \Delta\Sigma_d = F + D, \quad (24)$$

$$a_8 = \Delta\Sigma_u + \Delta\Sigma_d - 2\Delta\Sigma_s = 3F - D, \quad (25)$$

where a_3 and a_8 denote nonsinglet combinations of the
first moments of the polarized parton distributions corresponding to nonsinglet q_3 and q_8 distributions,

$$q_3 = (\delta u + \delta\bar{u}) - (\delta d + \delta\bar{d}), \quad (26)$$

$$q_8 = (\delta u + \delta\bar{u}) + (\delta d + \delta\bar{d}) - 2(\delta s + \delta\bar{s}). \quad (27)$$

A new reanalysis of F and D parameters with updated β-decay constants acquired [72] $F = 0.464 \pm 0.008$ and $D = 0.806 \pm 0.008$, so we make use of these evaluations in our present analysis; however, since we do not focus on flavor symmetry and we have $\delta\bar{u} \neq \delta\bar{d} \neq \delta s$, we can use the combination of Eqs. (24) and (25) as follows:

$$\Delta u + \Delta\bar{u} = 0.9275 + \Delta s + \Delta\bar{s},$$
$$\Delta d + \Delta\bar{d} = -0.3415 + \Delta s + \Delta\bar{s}, \quad (28)$$

and we apply the above relations in the analysis, so we exclude the parameters, define the first moment of $(\delta u + \delta\bar{u})$ and $(\delta d + \delta\bar{d})$ (i.e., $\eta_{u+\bar{u}}$ and $\eta_{d+\bar{d}}$) from the analysis, and obtain them by Eq. (28). The effect of symmetry breaking on the first moment of PPDFs has been discussed in detail in the literature [54,73].

C. Evolution and computational method

For numerical calculations, we need the scale evolution of the PPDFs from input scale Q_0^2 to each of the scales related to the data points. This evolution is done by a well-known set of integro-differential equations [74,75] that can be easily solved analytically after a transformation from x space to Mellin N-moment space. The Mellin transform of a generic function f depending on momentum fraction x is defined as

$$f(N) \equiv \int_0^1 x^{N-1} f(x) dx. \quad (29)$$

The transformation (29) has the pleasant applied property that convolutions change to ordinary products, which veritably simplifies calculations based on Mellin moments,

$$[f \otimes g](N) \equiv \int_0^1 dx^{n-1} \int_z^1 \frac{dy}{y} f\left(\frac{x}{y}\right) g(y) = f(N) g(N). \quad (30)$$

It can be performed analytically not only for the relevant splitting functions governing the evolution of the PDFs, but even for the partonic cross sections for both DIS and semi-inclusive DIS. The Mellin transform of the parton distributions q is defined similarly to Eq. (29):

$$\delta q(N, Q_0^2) = \int_0^1 x^{N-1} \delta q(x, Q_0^2) dx = \eta_q \mathcal{N}_q \left(1 + d_q \frac{N - 1 + a_q}{N + a_q + b_q}\right) \times B(N - 1 + a_q, b_q + 1) + c_q B\left(N + a_q - \frac{1}{2}, b_q + 1\right), \quad (31)$$

where $q = \{u + \bar{u}, d + \bar{d}, \bar{u}, \bar{d}, s, g\}$ and B denotes the Euler beta function.

The inverse Mellin transform reads

$$f(x) \equiv \frac{1}{2\pi i} \int_{\mathcal{C}_N} x^{-N} f(N) dN. \quad (32)$$

Note that $\mathcal{C}_N$ is an appropriate contour in the complex N plane which has an imaginary part with a range from $-\infty$ to $+\infty$ and which crosses the real axis to the right of the rightest pole of $f(N)$ [34].

Currently, in the case of using asymmetry data of SIDIS [49,54], which depends on two scaling variables x and z according to Eqs. (17) and (18), Mellin transformation and the inverse of that require straight extensions of Eqs. (29) and (32) to double the transformations, as was presented in Refs. [50,76,77].

Now for simplification of the double convolution in Eq. (17), we apply a method to change it to a single routine convolution by transforming the coefficients $\delta C_{ij}(x,z)$ from x-z space to N-z space,

$$\int_0^1 x^{N-1}\delta C_{ij}(x,z)dx = \delta C_{ij}(N,z), \tag{33}$$

and then we compute

$$\int_{0.2}^1 \delta C_{ij}(N,z) \otimes D_{i(j)}(z) = \delta\tilde{C}_{ij}(N). \tag{34}$$

Finally, we could have the evolution of NLO correction terms of g_{1N}^h in N-moment space according to Eqs. (17) and (30):

$$\begin{aligned} g_{1N}^h(N) = \frac{1}{2}\sum_{q,\bar{q}}^{n_f} e_q^2 \Bigg\{ & \int_{0.2}^1 dz\delta q D_q^h + \frac{\alpha_s(Q^2)}{2\pi}\delta q(N)\delta\tilde{C}_{qq}(N) \\ & + \frac{\alpha_s(Q^2)}{2\pi}\delta q(N)\delta\tilde{C}_{gq}(N) \\ & + \frac{\alpha_s(Q^2)}{2\pi}\delta g(N)\delta\tilde{C}_{qg}(N)\Bigg\}. \end{aligned} \tag{35}$$

The process is the same for Eq. (18). We calculate the transformation of Eq. (33) for all $C_{ij}(x,z)$ and $\delta C_{ij}(x,z)$ and provide them in the Appendix.

IV. TARGET MASS AND HIGHER TWIST CORRECTIONS

As shown in Table I, a considerable amount of data are at low Q^2 ($1 \le Q^2 \le 5$) and large x region, especially the CLAS data set for the proton and deuteron. The inclusion of nonperturbative corrections such as target mass correction (TMC) and dynamical higher twist (HT) terms might become important in this region, and considerable progress has been made in some recent analyses [23,49,70]. Despite the remarkable improvements of TMC and HT corrections, more detailed and precise investigations of the correcting terms for the polarized DIS structure function is still needed [78–80], and the polarized SIDIS correcting terms are not known completely yet.

Although our current purpose is the QCD analysis on DIS and SIDIS asymmetries without any correction, and we find an almost good description of all data sets without their inclusion, we perform an extra analysis considering correcting terms in order to study the effect of current reachable TMC and HT corrections on PPDFs. The comparison of the results is presented in Sec. VI.

An almost full description of the polarized DIS structure function reads

$$g_1(x,Q^2) = g_1^{\mathrm{TMC}}(x,Q^2) + g_1^{\mathrm{HT}}(x,Q^2), \tag{36}$$

where g_1^{TMC} is the polarized structure function including TMC and is given by [23,81]

$$\begin{aligned} g_1^{\mathrm{TMC}}(x,Q^2) = & \frac{x}{\xi}\frac{g_1(\xi,Q^2)}{(1+4M^2x^2/Q^2)^{3/2}} + \frac{4M^2x^2}{Q^2} \\ & \times \frac{x+\xi}{\xi(1+4M^2x^2/Q^2)^2}\int_\xi^1 \frac{d\xi_1}{\xi_1} g_1(\xi_1,Q^2) \\ & - \frac{4M^2x^2}{Q^2}\frac{2-4M^2x^2/Q^2}{2(1+4M^2x^2/Q^2)^{5/2}} \\ & \times \int_\xi^1 \frac{d\xi_1}{\xi_1}\int_{\xi_1}^1 \frac{d\xi_2}{\xi_2} g_1(\xi_2,Q^2), \end{aligned} \tag{37}$$

where M is the nucleon mass and

$$\xi = \frac{2x}{1+(1+4M^2x^2/Q^2)^{1/2}} \tag{38}$$

is called the Natchmann variable.

Since the dynamical higher twist contribution is not known with a thorough description yet, a phenomenological approach is used to determine the correcting HT terms. One can consider a spline function $h(x)$ in the HT correcting terms [23,49,70]

$$g_1^{\mathrm{HT}}(x,Q^2) = \frac{h(x)}{Q^2}, \tag{39}$$

with the knots at $x = 0.1$, 0.3, 0.5, and 0.7, and the $h(x)$ parameters for each knot are determined through the fit procedure simultaneously.

V. DETERMINATION OF MINIMUM χ^2 AND ERRORS

A. Minimization of χ^2

The process of global QCD analysis is based on the minimization of effective χ^2 which shows the quality of the fit carried out on data sets by variation of the input set of parameters. We use the QCD-PEGASUS program [82] for the evolution of distributions in N-moment space and the MINUIT package [83] for the minimization of the χ^2 function

$$\chi^2 = \sum_i \left(\frac{A_{1,i}^{\mathrm{exp}} - A_{1,i}^{\mathrm{theor}}}{\Delta A_{1,i}^{\mathrm{exp}}}\right)^2, \tag{40}$$

where $A_{1,i}^{\mathrm{exp}}$, $\Delta A_{1,i}^{\mathrm{exp}}$, and $A_{1,i}^{\mathrm{theor}}$ are the experimental measured value, the experimental uncertainty, and the theoretical value

for the ith data point, respectively. For the experimental error calculation, the statistical and systematic errors of each data point are added in quadrature. Currently, available SIDIS data are not precise enough to determine a strong coupling constant at input scale, so according to the precise scale dependent equation of $a_s = \frac{\alpha_s}{4\pi}$ used in PEGASUS in NLO [82],

$$\frac{1}{a_s(Q^2)} = \frac{1}{a_s(Q_0^2)} + \beta_0 \ln\left(\frac{Q^2}{Q_0^2}\right) - b_1 \ln\left\{\frac{a_s(Q^2)[1 + b_1 a_s(Q_0^2)]}{a_s(Q_0^2)[1 + b_1 a_s(Q^2)]}\right\}. \quad (41)$$

We fixed $\alpha_s(Q_0^2) = 0.580$ which corresponds to $\alpha_s(M_Z^2) = 0.119$, obtained from MRST02 analysis [69]. In Eq. (41), we have

$$\beta_0 = 11 - \frac{2}{3}n_f, \qquad \beta_1 = 102 - \frac{38}{3}n_f, \qquad b_1 = \frac{\beta_1}{\beta_0}. \quad (42)$$

Finally, we minimize the χ^2 with the 17 unknown parameters. We work at NLO in the fixed-flavor number scheme $n_f = 3$ in the QCD evolution with massless partonic flavors.

B. The neighborhood of χ_0^2 and error determination via Hessian method

Here we just present the essential points for studying the neighborhood of χ_0^2 and the full procedure is provided in Refs. [69,84,85]. As mentioned in Sec. V, we find the appropriate parameter set which minimizes the global χ^2 function; we call this PDF set S_0 and the parameter values of S_0, i.e., $p_1^0 \ldots p_n^0$, will be presented in Sec. VI.

By moving the parameters away from their obtained values, χ^2 increases by the amount of $\Delta\chi^2$,

$$\Delta\chi^2 = \chi^2 - \chi_0^2 = \sum_{i,j=1}^{d} H_{ij}(p_i - p_i^0)(p_j - p_j^0), \quad (43)$$

where the Hessian matrix H_{ij} is defined by

$$H_{ij} = \frac{1}{2}\frac{\partial^2\chi^2}{\partial p_i \partial p_j}\bigg|_{\min}, \quad (44)$$

and we note $C \equiv H^{-1}$. Now it is convenient to work in terms of eigenvalues and orthogonal eigenvectors of the covariance matrix,

$$\sum_{j=1}^{n} C_{ij} v_{jk} = \lambda_k v_{ik}. \quad (45)$$

Also, the displacement of parameter p_i from its minimum p_i^0 can be expressed in terms of rescaled eigenvectors $e_{ik} = \sqrt{\lambda_k} v_{ik}$,

$$p_i - p_i^0 = \sum_{k=1}^{n} e_{ik} z_k. \quad (46)$$

Putting Eq. (46) in (43) and considering the orthogonality of v_{ik}, we have

$$\Delta\chi^2 = \sum_{k=1}^{n} z_k^2. \quad (47)$$

Now the relevant neighborhood of χ^2 is the interior of the hypersphere with radius T:

$$\sum_{k=1}^{n} z_k^2 \le T^2, \quad (48)$$

and the neighborhood parameters are given by

$$p_i(s_k^{\pm}) = p_i^0 \pm t e_{ik}, \quad (49)$$

where s_k is the kth set of PDF and t adapted to make the desired $T = (\Delta\chi^2)^{\frac{1}{2}}$ and $t = T$ in the quadratic approximation. In Sec. VI, we present the dependence of $\Delta\chi^2$ along some random samples of eigenvector directions to test the quadratic approximation of Eq. (43).

Now we accompany the construction of the QCD fit with a reliable estimation of uncertainty. As discussed in Refs. [69,84,85], the master equation to obtain the uncertainties of observables in the modified Hessian method is

$$\Delta F = \frac{1}{2}\left[\sum_{k=1}^{n} (F(s_k^+) - F(s_k^-))^2\right]^{\frac{1}{2}}, \quad (50)$$

where $F(s_k^+)$ and $F(s_k^-)$ are the values of F extracted from the input set of parameters $p_i(s_k^{\pm})$ instead of p_i^0 mentioned in Eq. (49). However, it has been pointed out by DSSV [54] that the modified Hessian method is known to work reasonably well in extractions of spin independent parton densities and it is found to fail in the case of helicity parton densities for tolerances larger than $\Delta\chi^2 = 1$. So we prefer to calculate the PPDFs' error band using the standard Hessian method which is more reliable in this case. As presented in Eqs. (31) and (35), the evolved polarized parton densities and structure functions are attributive functions of the input parameters obtained in the QCD fit procedure at the scale Q_0^2; then their uncertainty can be written applying the standard Hessian method,

$$\Delta F = \left[\Delta\chi^2 \sum_{i,j=1}^{k} \frac{\partial F}{\partial p_i} C_{ij} \frac{\partial F}{\partial p_j}\right]^{\frac{1}{2}}. \quad (51)$$

TABLE II. Final parameter values and their statistical errors at the input scale $Q_0^2 = 1$ GeV^2; those parameters marked with (*) are fixed.

Flavor	η	a	b	c	d
$u+\bar{u}$	0.783	0.409 ± 0.0025	2.733 ± 0.0368	0.0*	80.855 ± 1.4115
$d+\bar{d}$	−0.485	0.123 ± 0.0036	4.249 ± 0.0280	0.0*	83.345 ± 13.9609
$\bar{u}$	0.051 ± 0.0022	0.409 ± 0.0025	10.0*	10.016 ± 13.5510	-32.424 ± 15.8386
$\bar{d}$	-0.081 ± 0.0020	0.123 ± 0.0036	10.0*	116.235 ± 81.2783	902.567 ± 615.0900
$\bar{s}$	-0.072 ± 0.0077	0.123 ± 0.0036	10.0*	0.0*	-16.045 ± 4.7815
g	-0.156 ± 0.0039	2.453 ± 0.0334	10.0*	0.0*	-3.922 ± 0.0659

Here we calculate the PPDFs' uncertainty with $\Delta\chi^2 = 1$ which is the most appropriate choice in the polarized case. If one wishes to choose $\Delta\chi^2 > 1$, one can simply scale our error bands by $(\Delta\chi^2)^{1/2}$.

VI. RESULTS

A. The quality of QCD fit

The values of obtained parameters attached to the input PPDFs are summarized in Table II. We find $\chi^2/\text{d.o.f.} = 1171.571/1132 = 1.03$ which yields an overlay acceptable fit to the experimental data; the individual χ^2 for each set of data is presented in Table I. There are some cases in which the deviation of $\chi^2/N_{\text{data}}^{(n)}$ from 1 is considerable; this is caused by the large fluctuation and irregularity of some of the data points in those cases. Since it was not possible to cover them in the fit, the value of $\chi^2/N_{\text{data}}^{(n)}$ grew undesirably.

The quality of the QCD fit to DIS and SIDIS asymmetry data is demonstrated in Figs. 3 and 4. Since we use large amounts of CLAS DIS data for the proton and deuteron [19] and they do not situate in the figure, we just show eight of them for presentation. As can be seen, the data are generally well described by the curves.

B. Extracted polarized parton distributions

In Fig. 5, we present the polarized parton distributions and their comparison to the results from DSSV09 [54], LSS10 [49], and NNPDFpol1.0 [20] at input scale $Q_0^2 = 1$ GeV^2. Since NNPDFpol1.0 is an unbiased analysis which is used only for inclusive DIS data, and they do not separate the quark and antiquark distributions, we consider the comparison of it and our model separately after the comparison with LSS10 and DSSV09.

Examining the $x(\delta u + \delta\bar{u})$ and $x(\delta d + \delta\bar{d})$ distributions, we see that all of the fits are in agreement. For the $x\delta\bar{u}$ and

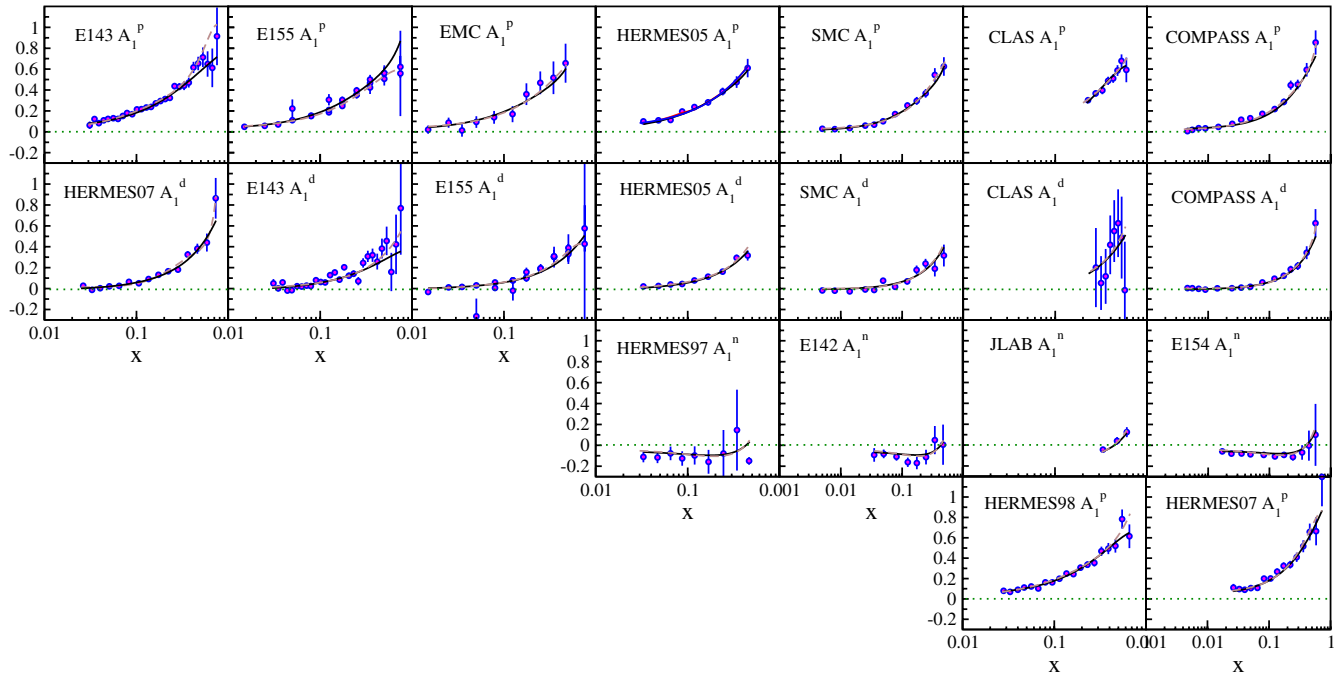

FIG. 3 (color online). Comparison of our NLO QCD results for the DIS asymmetries of the proton, neutron, and deuteron (solid line) with the data at measured x and Q^2. The dashed line is DIS asymmetry with TMC and HT corrections.

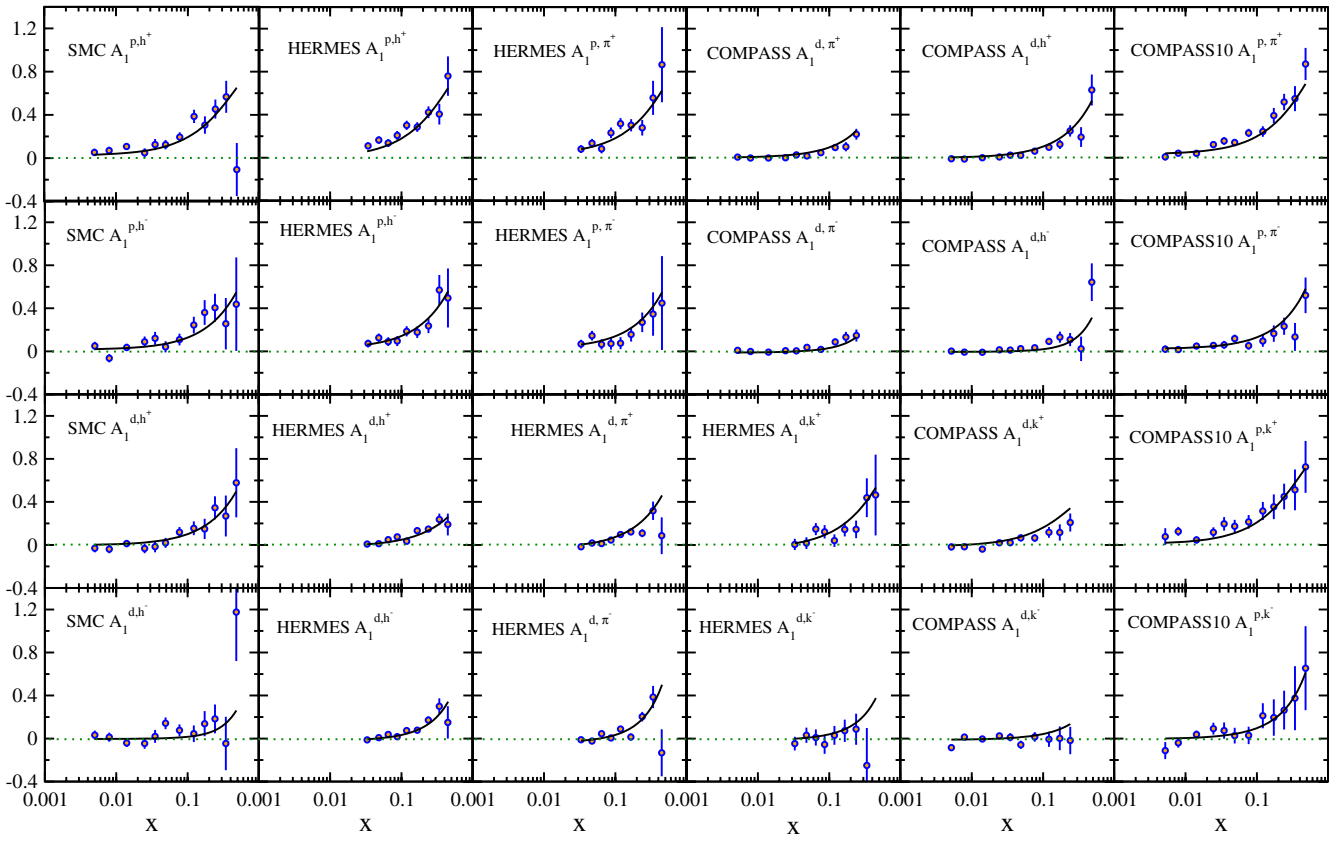

FIG. 4 (color online). Comparison of our NLO QCD results for the SIDIS asymmetries with the data at measured x and Q^2.

$x\delta\bar{d}$ distributions, the curves, especially our model and DSSV09, are very close; $\delta\bar{d}$ is negative for any x in the measured x region, while $\delta\bar{u}$ passes zero around $x = 0.1$–0.2 and becomes negative for large x for all three models. For the strange sea-quark density $x\delta s$, the main difference between the presented model, LSS10, and DSSV09 sets is that for $x < 0.03$, LSS10 is less negative than the others; also, both the current model and LSS10 are less positive than DSSV09 for $x > 0.03$. The other differences for the distributions come from the fact that both the DSSV09 and LSS10 analyses use a different number of data (we use the most and the newest ones), and DSSV09 uses pp collision data from RHIC which can impose individual effects on the parton distributions in the nucleon [54].

Generally, the QCD analyses on polarized high energy experiments apply some extra constraints on parameter space, such as DSSV09, LSS10, and our model. The main reason is that the available experimental data do not fully cover the kinematics ranges and the behavior of PPDFs should be controlled. Recently, NNPDF performed QCD analysis on polarized inclusive DIS data [20] and determined a new set of polarized PPDFs based on a Monte Carlo approach. As they mentioned, the neural networks are used as unbiased interpolants in their analysis. As shown in Fig. 5, $x(\delta u + \delta\bar{u})$ and $x(\delta d + \delta\bar{d})$ of NNPDFpol1.0 are almost comparable with other models, but the polarized strange sea-quark density $x\delta s$ is considerably different. The main cause of the difference between the sea quarks' behavior is that NNPDF used only inclusive DIS data and they do not have enough information to separate the quark and antiquark distributions. The polarized gluon distribution of NNPDFpol1.0 is almost compatible with zero for $x > 0.01$ values, so one can conclude that the theoretical constraints on the polarized distribution and the choice of parametrization form have a considerable effect on the gluon behavior. In addition, we understand that the role of the polarized gluon distribution in the spin structure of the nucleon is not known well, and theoretical constraints have direct effects on the results from different analyses. Also, including more high energy data sets from different types of polarized experiments can release the polarized gluon distribution from extra assumptions. The effect of SIDIS data and symmetry breaking on polarized gluon behavior will be discussed more in Sec. VI E.

C. The impact of SIDIS data in determining the polarized sea-quark distributions

Generally speaking, polarized inclusive DIS data cannot distinguish $\delta\bar{u}$, $\delta\bar{d}$, and $\delta\bar{s}$, but $\delta\bar{u} = \delta\bar{d} = \delta s = \delta\bar{s} = \delta\bar{q}$ is well determined and all the standard scenario NLO QCD analyses yield a negative value of it for any x in the

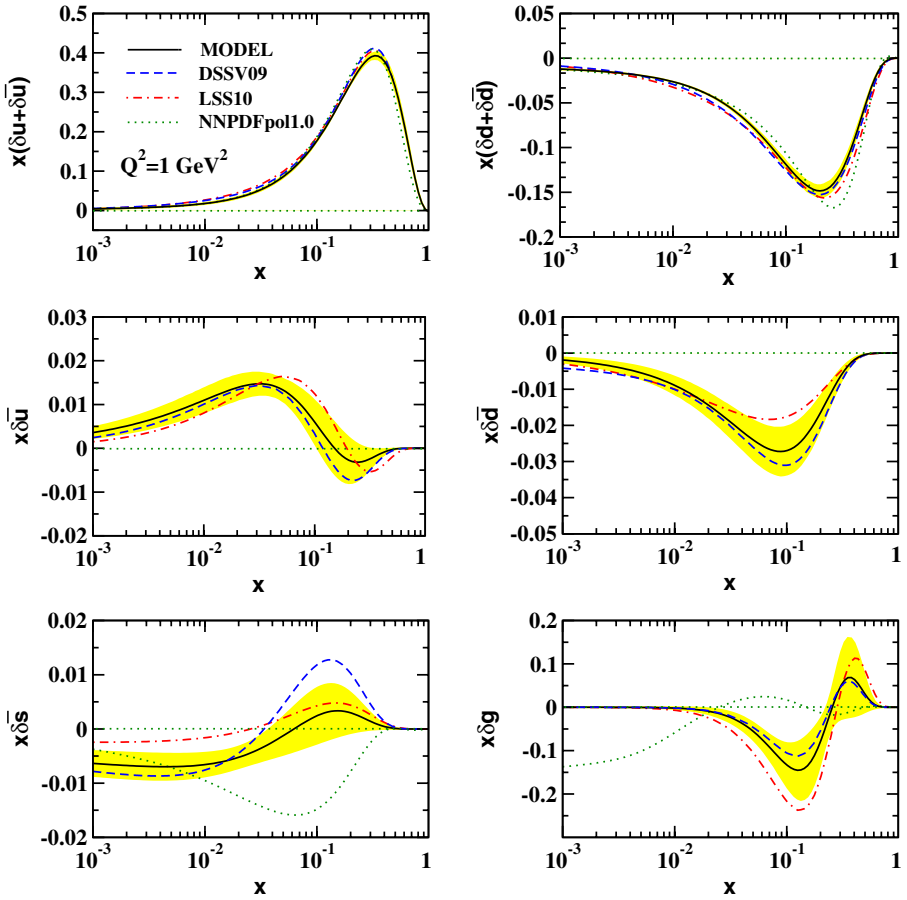

FIG. 5 (color online). The result of our analysis for quark helicity distributions at $Q_0^2 = 1$ GeV^2 in comparison with DSSV09 [54], LSS10 [49], and unbiased NNPDFpol1.0 [20].

measured region [23]. Employing SIDIS data, a flavor decomposition of the polarized sea quarks is obtained and the light antiquark polarized densities $\delta\bar{u}$, $\delta\bar{d}$, and $\delta s = \delta\bar{s}$ are determined separately. Figure 6 shows the difference between $\delta\bar{u}$, $\delta\bar{d}$ in the current analysis compared to other models and experimental data.

Also, in the present parametrization we use a term $(1 + c_s x^{0.5} + d_s x)$ in the input strange sea-quark distribution to let a sign change for $\delta s = \delta\bar{s}$, which was not considered in the standard scenario [21]. The comparison of polarized light sea-quark distributions $(x\delta s, x\delta\bar{u}, x\delta\bar{d})$ in the standard scenario and current model are presented in Fig. 7. It shows that the behavior of the polarized strange-quark density remains puzzling [86].

Note that by having SIDIS data, δs and $\delta\bar{s}$ can be separately determined as was done recently by the COMPASS Collaboration [56]. However, it was demonstrated that there is no considerable difference between δs and $\delta\bar{s}$ in the x range covered by their data. Also, the errors of the presented values of the difference $\delta s(x) - \delta\bar{s}(x)$ are quite large to allow us to conclude the assumption $\delta s(x) = \delta\bar{s}(x)$ like LSS10 and DSSV09. So, the above assumption and also the form of the fragmentation functions used to extract PPDFs by different groups may be possible causes of the contradiction between sea-quark densities obtained from the analyses of inclusive DIS data and combined inclusive and semi-inclusive DIS data sets [86].

D. The effect of COMPASS SIDIS data on polarized sea-quark distributions

As shown in Table I, the measurement of the SIDIS asymmetries for unidentified charged hadrons was performed by the SMC Collaboration. Then the SIDIS asymmetries data for charged pion production from a proton target and for charged kaon and pion production from a deuteron target were reported by HERMES. These asymmetries were used in most DIS and SIDIS QCD analyses, but the SIDIS asymmetry data from COMPASS are partially employed, especially the new semi-inclusive COMPASS asymmetries data for scattering of muons from a polarized proton target for identified charged pion and kaon production, $A_1^{p,\pi^\pm}$ and $A_1^{p,k^\pm}$ [56], which were not available for the analysis before 2010.

In order to study the effect of COMPASS SIDIS data on polarized parton distributions, we show the comparison of our PPDF results extracted from all data sets in Table I, and the PPDF results extracted by excluding COMPASS SIDIS

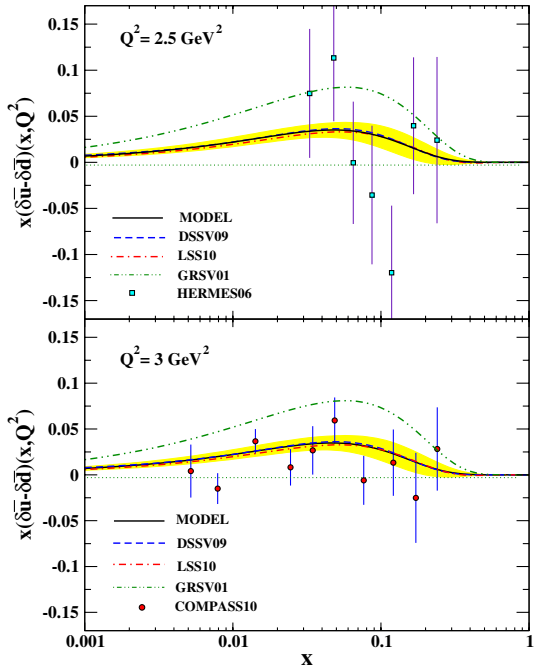

FIG. 6 (color online). The quark helicity distributions for the difference $x(\delta\bar{u} - \delta\bar{d})$ at $Q^2 = 2.5$ and 3 GeV^2 compared to DSSV09 [54], LSS10 [49], GRSV01 [31], and experimental data [15,56].

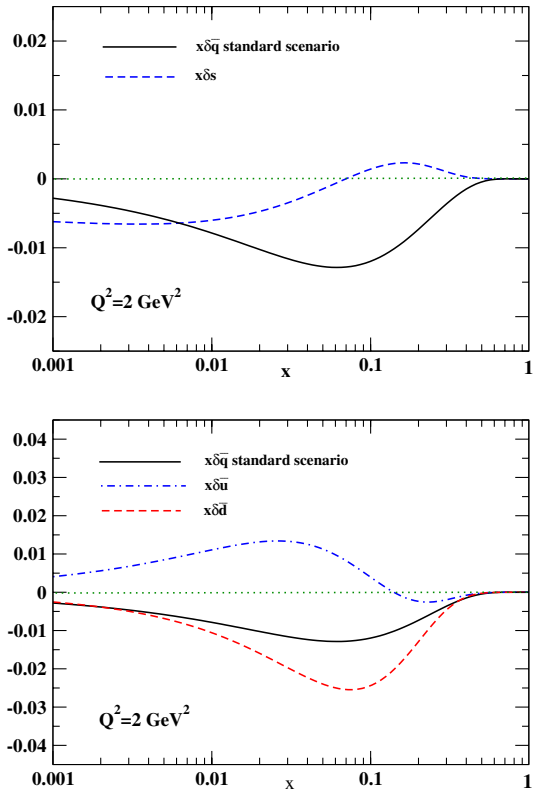

FIG. 7 (color online). The quark helicity distributions for $x\delta s$, $x\delta\bar{u}$, and $x\delta\bar{d}$ at $Q_0^2 = 2$ GeV^2 compared to $x\delta q$, obtained from the previous standard scenario [21].

data sets in Fig. 8. As can be seen, COMPASS data have an effect on $\delta\bar{u}$, $\delta\bar{d}$, and $\delta s = \delta\bar{s}$ distributions since $\pi^{\pm}$ and $k^{\pm}$ are directly related to them. The changes of sea-quark distributions are considerable in the $0.07 \leq x \leq 0.4$ region that is well covered by the new COMPASS data. The distributions of $\delta u + \delta\bar{u}$, $\delta d + \delta\bar{d}$, and δg are not changed considerably.

E. Gluon polarization

In order to study the effect of SIDIS data on polarized gluon distribution, we perform another analysis with positive polarized gluon distribution. We understand that utilizing polarized DIS and SIDIS data in the QCD analysis can not enforce the positive or sign changing polarized gluon distributions and the data cannot distinguish between these two scenarios, although the recent analyses which employ both DIS and SIDIS data (and not pp collision data) could extract sign changing $x\delta g$ [49,87]. In Table III we present the values of obtained parameters in the positive gluon scenario. We find $\chi^2/\text{d.o.f} = 1.02$ which is almost equal to the one obtained from the sign changing gluon scenario $\chi^2/\text{d.o.f} = 1.03$. Figure 9 shows the comparison of PPDFs extracted from positive and sign changing gluon scenarios. As can be seen, all the distributions are almost not changed except $x\delta g$. Figure 10 shows the gluon distribution comparison between our previous standard scenario and the present sea flavor decomposition analysis. As presented, SU(2) and SU(3) symmetry breaking has a direct effect on $x\delta g(x, Q^2)$ and makes it less. The gluon results of other models of both standard and light sea-quark decomposition scenarios are also presented in Fig. 10, and they confirm this effect too [21,23,31,49,54]. We also calculated the ratio $\delta g/g$, using our extracted PPDFs for polarized gluon distributions and MRST02 [69] NLO QCD analysis for unpolarized gluon distributions. In Fig. 11, we present a comparison for $\delta g/g$ from LSS10, DSSV09, and our models (sign changing and positive gluon scenarios) at $Q^2 = 3$ GeV^2 with measured values from experimental data [88–92]. Although we do not use the mentioned data in the current analysis, our results can predict the data very well.

F. The effect of TMC and HT corrections

The polarized DIS structure function presented in Eq. (16) is corrected by TMC and HT terms as presented in Eq. (36) in Sec. IV. To see the effect of the correcting terms, we reperform the analysis using Eq. (36) in DIS asymmetry presented in Eq. (14). We also add ten higher twist parameters for the proton and neutron, introduced in Eq. (39), to the unknown parameters of the fitting procedure. The values of extracted parameters and HT terms are shown in Tables IV and V, respectively. We find $\chi^2/\text{d.o.f.} = 1.01$ which is a little less than the one obtained from the QCD fit without the correction and shows that DIS asymmetry data are slightly better described by including correction terms. The obtained DIS asymmetries are shown

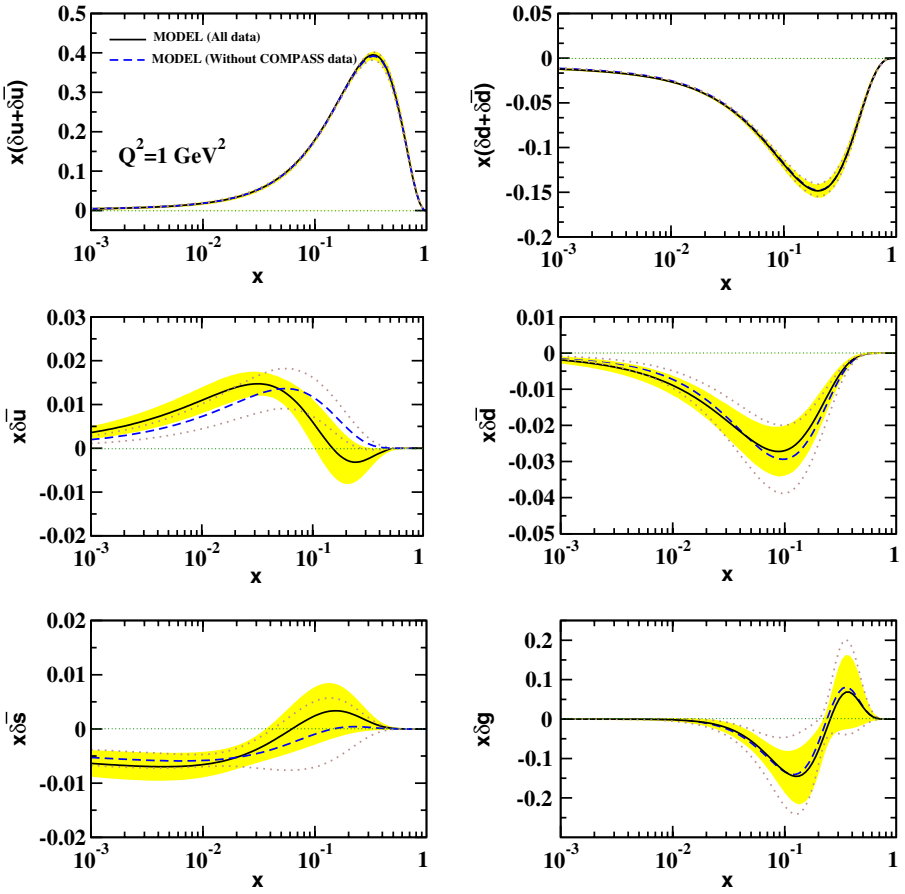

FIG. 8 (color online). The comparison of PPDF results extracted from all data sets shown in Table I, and the PPDF results extracted by excluding COMPASS SIDIS data sets at $Q_0^2 = 1$ GeV^2. The corresponding error bands of them are also shown.

in Fig. 3 in comparison with asymmetries without corrections, as we expect some of them are lightly changed at large x region.

The extracted PPDFs are compared to our model (without the corrections) in Fig. 12. As can be seen, the effect of TMC and HT is not remarkable since the corrections are small and they are just applied on DIS data. The change of PPDFs is negligible at small x values and lightly grows at higher x values for $x(\delta u + \delta\bar{u})$ and $x(\delta d + \delta\bar{d})$. Also, the magnitudes of the maximum and minimum of the functions become slightly larger.

G. Behavior of $\Delta\chi^2$

For more deliberation, in the preliminary QCD fit process we let all input parameters vary. While investigating the behavior of $\Delta\chi^2$, we observe that χ^2 increases consumedly in some points and a big amount of redundance in parameters happens; this redundancy results in disorder of quadratic behavior of $\Delta\chi^2$. In order to have the Hessian method work as shown in Sec. V B, we fix some parameters at their best obtained value so that the Hessian matrix depends on the number of parameters which are independent sufficiently for the quadratic behavior of $\Delta\chi^2$;

TABLE III. Final parameter values and their statistical errors at the input scale $Q_0^2 = 1$ GeV^2 for the positive gluon scenario; those parameters marked with (*) are fixed.

Flavor	η	a	b	c	d
$u + \bar{u}$	0.770	0.411 ± 0.0955	2.760 ± 0.1356	0.0*	78.145 ± 39.9149
$d + \bar{d}$	−0.498	0.125 ± 0.0080	4.221 ± 0.0359	0.0*	67.151 ± 4.0270
$\bar{u}$	0.051 ± 0.0004	0.411 ± 0.0955	10.0*	11.231 ± 0.4776	-32.425 ± 0.6351
$\bar{d}$	-0.081 ± 0.0003	0.125 ± 0.0080	10.0*	85.423 ± 2.4403	915.221 ± 26.7240
$\bar{s}$	-0.079 ± 0.0387	0.125 ± 0.0080	10.0*	0.0*	-15.843 ± 3.2887
g	0.081 ± 0.0008	3.958 ± 0.0326	10.0*	0.0*	25.820 ± 0.8029

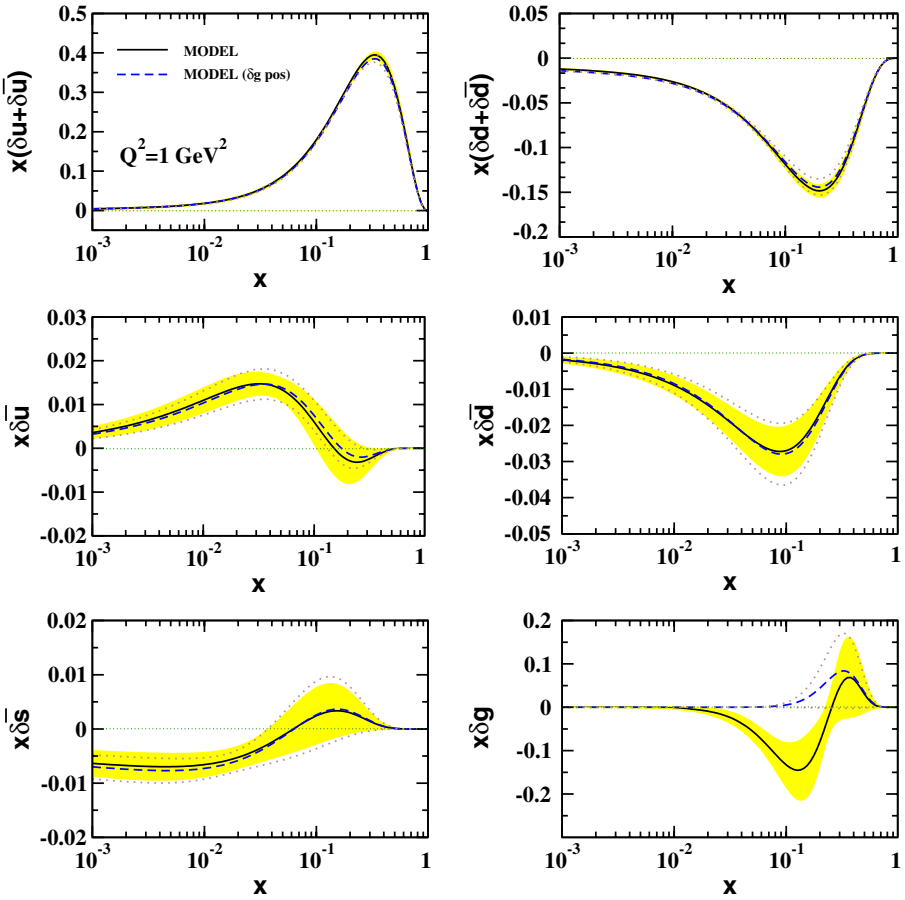

FIG. 9 (color online). The comparison of PPDF results extracted from sign changing and positive gluon scenarios at $Q_0^2 = 1$ GeV^2. The corresponding error bands of them are also shown.

the detailed fixing and constraints in parameter space were discussed in Secs. III B and V.

To test the quadratic approximation in Eq. (43), Fig. 13 presents $\Delta\chi^2$ along some random samples of eigenvector directions and eigenvalues, $k = 1, 7, 9, 15$. The curves for middle values of $\lambda_{k=7,9}$ are very close to the ideal quadratic curve $\Delta\chi^2 = t^2$, and for other eigenvalues $\lambda_{k=1,15}$ we see some departure from the ideal quadratic curve, which shows that the quadratic approximation is almost adequate, though imperfect. The behavior of the same odd curves which are also available in the other QCD analysis [84] usually correspond to the parameters controlling some unknown x dependence parts of sea-quark and gluon densities.

H. The spin sum rule

In the framework of QCD, the spin $\frac{1}{2}$ of the proton can be defined in terms of the first moment of the total quark and gluon polarized densities and their orbital angular momentum,

$$\frac{1}{2} = \frac{1}{2}\Delta\Sigma^p + \Delta g^p + L_z^p, \tag{52}$$

where L_z^p contains the total orbital angular momentum of all partons. The contribution of $\frac{1}{2}\Delta\Sigma + \Delta g$ in the scale of $Q^2 = 4$ GeV^2 is around 0.010 in the present analysis. The reported values from DSSV09 [54] and LSS10 [49] are 0.026 and -0.212, respectively. For the positive gluon

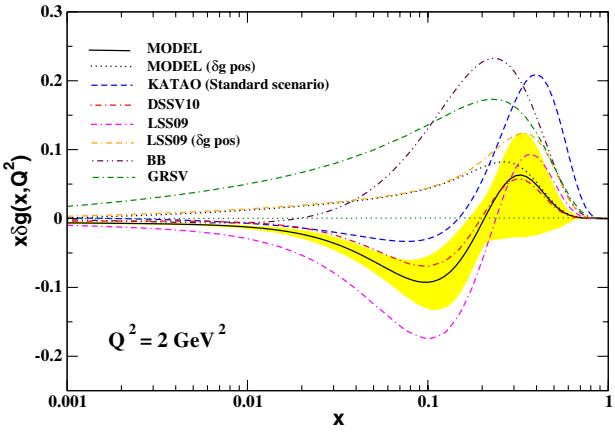

FIG. 10 (color online). The gluon helicity distributions at $Q^2 = 2$ GeV^2 compared to the symmetry breaking [49,54] and standard scenario [21,23,31] analyses.

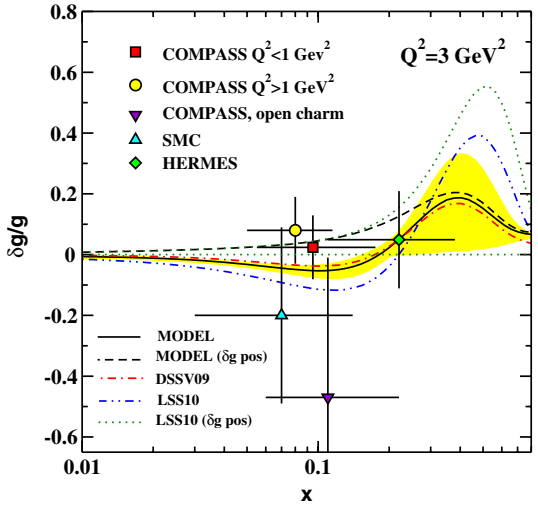

FIG. 11 (color online). The calculated ratio $\delta g/g$ for DSSV, LSS [49,54], and our model in comparison with experimental data from COMPASS, HERMES, and SMC [88–92] at $Q^2 = 3$ GeV^2.

scenario, LSS obtained 0.419 while our result is 0.367. In Table VI we compare the values of polarized PDFs' first moment in NLO approximation with other recent analyses. Since the values of $\frac{1}{2}\Delta\Sigma$ are almost comparable, we observe and conclude that the difference between the reported values of $\frac{1}{2}\Delta\Sigma + \Delta g$ must be caused by different gluon distributions. Indeed, proliferation in PPDF data for sea quarks from SIDIS experiments eventuates to more accurate results for gluon distribution than the analysis on DIS data only, so one cannot yet come to a definite conclusion about the contribution of the orbital angular momentum to the total spin of the proton. The estimation of the valence spin distribution can be written as an accurate relation obtained from inclusive interactions in the experiments. Indeed, one obtains the following at LO [93]:

$$\delta u_v + \delta d_v \sim \frac{36}{5}\frac{g_1^d}{(1-1.5\omega_D)}, \tag{53}$$

which is approximately true at NLO.

Theoretically, the first moment of the polarized valence distributions, truncated to the measured range of x,

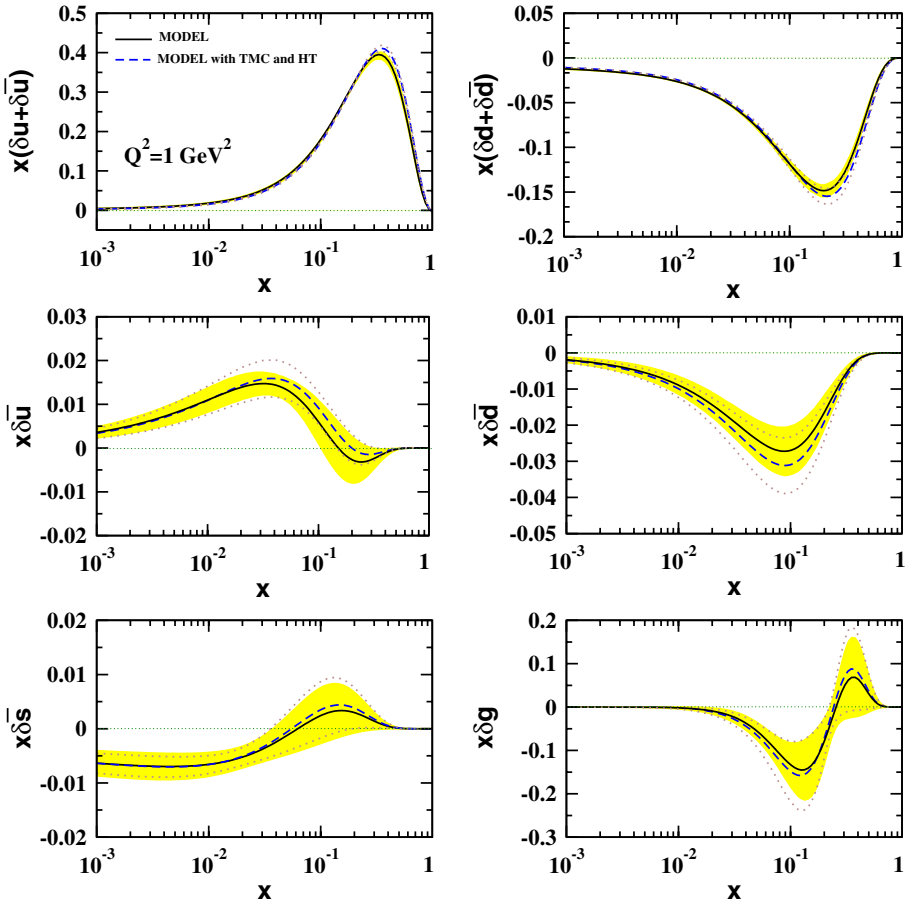

FIG. 12 (color online). The comparison of PPDF results extracted from the model and the PPDF results extracted by including TMC and HT at $Q_0^2 = 1$ GeV^2. The corresponding error bands of them are also shown.

TABLE IV. Final parameter values and their statistical errors at the input scale $Q_0^2 = 1$ GeV^2, considering TMC and HT corrections; those parameters marked with (*) are fixed.

Flavor	η	a	b	c	d
$u+\bar{u}$	0.796	0.411 ± 0.0014	2.554 ± 0.0050	0.0*	98.625 ± 2.4400
$d+\bar{d}$	-0.427	0.135 ± 0.0017	3.995 ± 0.1499	0.0*	87.252 ± 1.4589
$\bar{u}$	0.056 ± 0.0060	0.411 ± 0.0014	10.0*	11.251 ± 14.5676	-30.224 ± 15.9715
$\bar{d}$	-0.091 ± 0.0026	0.135 ± 0.0017	10.0*	133.343 ± 12.1680	1022.645 ± 200.5183
$\bar{s}$	-0.065 ± 0.0039	0.135 ± 0.0017	10.0*	0.0*	-18.185 ± 3.0677
g	-0.161 ± 0.0060	2.413 ± 0.0236	10.0*	0.0*	-4.122 ± 0.0201

TABLE V. The higher twist parameters $h_p(x)$ and $h_n(x)$ extracted for four knots at 0.1, 0.3, 0.5, and 0.7.

x	$h_p(x)$	$h_n(x)$
0.1	0.008 ± 0.003	0.022 ± 0.001
0.3	-0.031 ± 0.001	0.028 ± 0.002
0.5	-0.052 ± 0.029	0.046 ± 0.015
0.7	-0.018 ± 0.004	0.018 ± 0.005

$$\Gamma_v(x_{\min} < x < x_{\max}) = \int_{x_{\min}}^{x_{\max}} [\delta u_v(x) + \delta d_v(x)]\mathrm{d}x, \quad (54)$$

is obtained and shown for the current model and DNS [52] in Table VII. We obtain for the full measured range of x in SMC [46], HERMES [15], and COMPASS [93] experiments

$$\Gamma_v(0.003 < x < 0.7) = 0.454, \quad (55)$$

$$\Gamma_v(0.023 < x < 0.6) = 0.445, \quad (56)$$

$$\Gamma_v(0.006 < x < 0.7) = 0.459, \quad (57)$$

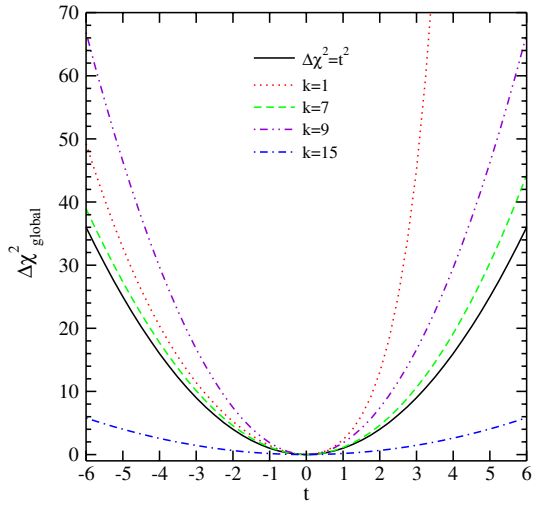

FIG. 13 (color online). $\Delta\chi^2_{\text{global}}$ as a function of t for some random sample eigenvectors.

TABLE VI. First moments of polarized PDFs at $Q^2 = 4$ GeV^2. The corresponding DSSV09 and LSS10 values are also presented.

Fit	$\Delta\bar{s}$	ΔG	$\Delta\Sigma$
DSSV09	-0.056	-0.096	0.245
LSS10 (δg pos)	-0.063	0.316	0.207
LSS10	-0.055	-0.339	0.254
MODEL	-0.042	-0.138	0.256
MODEL (δg pos)	-0.046	0.245	0.244

at $Q^2 = 10$, 2.5, and 10 GeV^2, respectively. Our value of Γ_v confirms the experimental results and the values come from DNS analysis.

An estimation of the sea-quark first moment contribution to the nucleon spin can be generated by combining the values of Γ_v, Γ_1^N, and a_8 [93],

$$\Delta\bar{u} + \Delta\bar{d} = 3\Gamma_1^N - \frac{1}{2}\Gamma_v + \frac{1}{12}a_8, \quad (58)$$

where Γ_1^N is defined as the first moment of polarized structure function g_1 for the average nucleon N in an isoscalar target $[g_1^N = (g_1^p + g_1^n)/2]$:

$$\Gamma_1^N(Q^2 = 10\ \text{GeV}^2) = \int_0^1 g_1^N(x, Q^2), \quad (59)$$

and $(a_8 = 3F - D)$ is evaluated from semileptonic hyperon decays. The result is reported to be zero for the COMPASS experiment, as shown in Table VII. The zero value of $\Delta\bar{u} + \Delta\bar{d}$ suggests that $\Delta\bar{u}$ and $\Delta\bar{d}$, if they are not zero, must have opposite signs. Previous estimations by SMC and HERMES are comparable with this supposition and are also given in Table VII. The DNS parametrization, like the present model, finds a positive value for $\Delta\bar{u}$ and a negative value for $\Delta\bar{d}$, almost equal in absolute value. Opposite signs of $\Delta\bar{u}$ and $\Delta\bar{d}$ are anticipated in several models, e.g., in Refs. [31,49,54]; see also [94] and references therein.

VII. SUMMARY

We have presented a NLO QCD analysis of the polarized DIS and SIDIS data on the nucleon. During the analysis, we considered the SU(2) and SU(3) symmetry breaking

TABLE VII. Evaluations of the first moments $\Delta u_v + \Delta d_v$ and $\Delta\bar{u} + \Delta\bar{d}$ from SMC [46], HERMES [15], and COMPASS [93] data and also from the DNS analysis [52] and present model truncated to the range of each relevant experiment. The SMC results were obtained with the assumption of a SU(3) symmetric sea: $\Delta\bar{u} = \Delta\bar{d} = \Delta\bar{s}$.

			$\Delta u_v + \Delta d_v$			$\Delta\bar{u} + \Delta\bar{d}$		
	x range	Q^2 (GeV^2)	Exp.Value	DNS	MODEL	Exp.Value	DNS	MODEL
SMC98	0.003–0.7	10	$0.26 \pm 0.21 \pm 0.11$	0.386	0.454	$0.02 \pm 0.08 \pm 0.06$	−0.009	−0.043
HERMES05	0.023–0.6	2.5	$0.43 \pm 0.07 \pm 0.06$	0.363	0.445	$-0.06 \pm 0.04 \pm 0.03$	−0.005	−0.040
COMPASS07	0.006–0.7	10	$0.40 \pm 0.07 \pm 0.06$	0.385	0.459	⋯	−0.007	−0.043
	0–1		$0.41 \pm 0.07 \pm 0.06$	⋯	⋯	$0.0 \pm 0.04 \pm 0.03$	⋯	⋯

scenario, i.e., $\delta\bar{u} \neq \delta\bar{d} \neq \delta\bar{s}$; since the available experimental data are not enough to distinguish δs from $\delta\bar{s}$, we took them to be equal: $\delta s = \delta\bar{s}$. The role of the semi-inclusive data in determining the polarized sea quarks was discussed and we have found also that the polarized gluon density is still ambiguous; this ambiguity is the main reason that the quark-gluon contribution into the total spin of the proton is still not well determined. We have also calculated the error of PPDFs by the standard Hessian method and investigated the quadratic behavior of $\Delta\chi^2$. Having extracted the polarized PDFs, we computed the first moments of them and discussed sum rules. In general, we have found good agreement with the experimental data, and our results are in accord with other determinations, especially DSSV09 and LSS10 which are the most precise ones. In conclusion, this demonstrates progress of the field toward a detailed description of the spin structure of the nucleon [87,95–99]. The results of our new analysis applying pp collision data and studying the impact of fragmentation functions on PPDFs will be presented in a separate publication very soon.

ACKNOWLEDGMENTS

We thank F. Olness for useful discussions and reading the manuscript. F. A. appreciates M. Stratmann from DSSV for kind orientation, E. Kabuss from the COMPASS Collaboration and D. Stamenov from LSS for communications and M. Goharipour from Semnan University for his kind help. A. N. K. thanks SITP (Stanford Institute for Theoretical Physics) for partial support and the Physics Department of SMU (Southern Methodist University) for their hospitality during the completion of this work. He is also grateful to CERN TH-PH division for the hospitality where a portion of this work was performed. This project was financially supported by Semnan University, Semnan University Science and Technology Park, and the School of Particles and Accelerators, Institute for Research in Fundamental Sciences (IPM).

APPENDIX A: FORTRAN CODE

A Fortran package containing our polarized parton distributions $x\delta u_v(x,Q^2)$, $x\delta d_v(x,Q^2)$, $x\delta g(x,Q^2)$, $x\delta\bar{u}(x,Q^2)$, $x\delta\bar{d}(x,Q^2)$, and $x\delta s(x,Q^2)$ at NLO in the $\overline{\text{MS}}$ scheme can be found online [100] or obtained via e-mail from the authors. These functions are interpolated using cubic splines in Q^2 and a linear interpolation in $\log(Q^2)$. The package includes an example program to illustrate the use of the routines.

APPENDIX B: N-MOMENT OF ALL POLARIZED SIDIS WILSON COEFFICIENTS

The transformation of Eq. (33) gives the SIDIS Wilson coefficients in N-z space:

$$
\begin{aligned}
C_{qq}(N,z) = C_f\Bigg\{ & -8\delta(1-z) + \tilde{P}_{qq}(z)\ln\frac{Q^2}{M^2} + L_1(z) + L_2(z) + (1-z) + \delta(1-z)\Bigg[\Bigg(\frac{1}{N} + \frac{1}{1+N} - 2\gamma - 2\Psi(N) - \frac{2}{N} \\
& - \frac{2}{N+1} + \frac{3}{2}\Bigg)\ln\frac{Q^2}{M^2} + \frac{1}{6}\Bigg(\frac{3}{N^2} + \frac{3}{(1+N)^2} + 6\gamma\Bigg(\gamma + \frac{1}{N} + \frac{1}{1+N}\Bigg) + \pi^2 + 3\Psi(N)\times(4\gamma + \Psi(N)) \\
& + 3\Psi^2(N+2) - 6\frac{d\Psi(N)}{dN}\Bigg) - \Bigg(-\frac{1}{N^2} + \frac{1}{(1+N)^2} - 2\zeta(2,N+1)\Bigg) + \frac{1}{N+N^2}\Bigg] - 2(\gamma + \Psi(N))\frac{1}{(1-z)_+} \\
& + (1+z)(\gamma + \Psi(N)) - \Bigg(\frac{1}{N} + \frac{1}{1+N}\Bigg)\frac{1}{(1-z)_+} + \frac{2(1+N+NZ)}{N+N^2} - \frac{2(1-z)}{N+N^2}\Bigg\},
\end{aligned}
\tag{B1}
$$

$$C_{gq}(N,z)=C_f\left\{\frac{1+(1-z)^2}{z}\left[\ln\left(\frac{Q^2}{M^2}z(1-z)\right)-\gamma\right]-\Psi(N)+z+2\frac{1+2N-Nz}{N+N^2}-\frac{1+2N}{Nz+N^2z}-\frac{2z}{N+N^2}\right\}, \quad \text{(B2)}$$

$$C_{qg}(N,z)=\frac{1}{2}\left\{\delta(1-z)\quad\left[-\frac{2-2N-(2+N+N^2)(\gamma+\Psi(N))}{N(1+N)(2+N)}+\frac{2}{2+3N+N^2}\right]+\frac{2+N+N^2}{2N+3N^2+N^3}\left[\frac{1}{(1-z)_+}+\frac{1}{z}-2\right]\right\}, \quad \text{(B3)}$$

$$\delta C_{qq}(N,z)=C^1_{qq}-2C_f\frac{1}{N+N^2}(1-z), \quad \text{(B4)}$$

$$\delta C_{qq}(N,z)=C^1_{qq}-2C_f\frac{1}{N+N^2}z, \quad \text{(B5)}$$

$$\delta C_{qg}(N,z)=\frac{1}{2}\left\{\delta(1-z)\left[-\frac{2+(N-1)(\gamma+\Psi(N))}{N(1+N)}\quad+\frac{2}{N+N^2}\right]\quad+\frac{N-1}{N(1+N)}\left[\frac{1}{(1-z)_+}+\frac{1}{z}-2\right]\right\}, \quad \text{(B6)}$$

where $C_f=4/3$, $\gamma\simeq 0.577216$ and

$$\tilde{P}_{qq}(z)=\frac{1+z^2}{(1-z)_+}+\frac{3}{2}\delta(1-z), \quad \text{(B7)}$$

$$L_1(z)=(1+z^2)\left(\frac{\ln(1-z)}{1-z}\right), \quad \text{(B8)}$$

$$L_2(z)=\frac{1+z^2}{1-z}\ln z, \quad \text{(B9)}$$

$$\int_0^1 dz f(z)(g(z))_+\equiv\int_0^1 dz[f(z)-f(1)]g(z). \quad \text{(B10)}$$

[1] J. Ashman *et al.* (European Muon Collaboration), Phys. Lett. B **206**, 364 (1988).
[2] J. Ashman *et al.* (European Muon Collaboration), Nucl. Phys. **B328**, 1 (1989).
[3] G. Altarelli, arXiv:0907.1751.
[4] M. Anselmino, A. Efremov, and E. Leader, Phys. Rep. **261**, 1 (1995); , Phys. Rep. **281**, 399(E) (1997).
[5] E. W. Hughes and R. Voss, Annu. Rev. Nucl. Part. Sci. **49**, 303 (1999).
[6] B. Lampe and E. Reya, Phys. Rep. **332**, 1 (2000).
[7] B. W. Filippone and X. D. Ji, Adv. Nucl. Phys. **26**, 1 (2001).
[8] B. Adeva *et al.* (Spin Muon Collaboration), Phys. Rev. D **58**, 112001 (1998).
[9] M. G. Alekseev *et al.* (COMPASS Collaboration), Phys. Lett. B **690**, 466 (2010); V. Y. Alexakhin *et al.* (COMPASS Collaboration), Phys. Lett. B **647**, 8 (2007).
[10] P. L. Anthony *et al.* (E142 Collaboration), Phys. Rev. D **54**, 6620 (1996).
[11] K. Abe *et al.* (E143 Collaboration), Phys. Rev. D **58**, 112003 (1998).
[12] K. Abe *et al.* (E154 Collaboration), Phys. Rev. Lett. **79**, 26 (1997).

[13] P. L. Anthony *et al.* (E155 Collaboration), Phys. Lett. B **493**, 19 (2000).
[14] P. L. Anthony *et al.* (E155 Collaboration), Phys. Lett. B **463**, 339 (1999).
[15] A. Airapetian *et al.* (HERMES Collaboration), Phys. Rev. D **71**, 012003 (2005).
[16] K. Ackerstaff *et al.* (HERMES Collaboration), Phys. Lett. B **404**, 383 (1997); A. Airapetian *et al.* (HERMES Collaboration), Phys. Lett. B **442**, 484 (1998).
[17] A. Airapetian *et al.* (HERMES Collaboration), Phys. Rev. D **75**, 012007 (2007).
[18] X. Zheng *et al.* (JLab/Hall A Collaboration), Phys. Rev. Lett. **92**, 012004 (2004); , Phys. Rev. C **70**, 065207 (2004).
[19] K. V. Dharmawardane *et al.* (CLAS Collaboration), Phys. Lett. B **641**, 11 (2006).
[20] R. D. Ball, S. Forte, A. Guffanti, E. R. Nocera, G. Ridolfi, J. Rojo (The NNPDF Collaboration), Nucl. Phys. **B874**, 36 (2013).
[21] A. N. Khorramian, S. A. Tehrani, S. T. Monfared, F. Arbabifar, and F. I. Olness, Phys. Rev. D **83**, 054017 (2011).
[22] T. Gehrmann and W. J. Stirling, Phys. Rev. D **53**, 6100 (1996).
[23] J. Blumlein and H. Bottcher, Nucl. Phys. **B841**, 205 (2010).
[24] G. Altarelli, R. D. Ball, S. Forte, and G. Ridolfi, Acta Phys. Pol. B **29**, 1145 (1998).
[25] R. D. Ball, G. Ridolfi, G. Altarelli, and S. Forte, arXiv:hep-ph/9707276.
[26] C. Bourrely, F. Buccella, O. Pisanti, P. Santorelli, and J. Soffer, Prog. Theor. Phys. **99**, 1017 (1998).
[27] L. E. Gordon, M. Goshtasbpour, and G. P. Ramsey, Phys. Rev. D **58**, 094017 (1998).
[28] E. Leader, A. V. Sidorov, and D. B. Stamenov, Phys. Lett. B **462**, 189 (1999); , Phys. Lett. B **445**, 232 (1998); , Phys. Rev. D **58**, 114028 (1998); , Int. J. Mod. Phys. A **13**, 5573 (1998).
[29] M. Stratmann, Nucl. Phys. B, Proc. Suppl. **79**, 538 (1999).
[30] D. K. Ghosh, S. Gupta, and D. Indumathi, Phys. Rev. D **62**, 094012 (2000).
[31] M. Gluck, E. Reya, M. Stratmann, and W. Vogelsang, Phys. Rev. D **63**, 094005 (2001).
[32] R. S. Bhalerao, Phys. Rev. C **63**, 025208 (2001).
[33] E. Leader, A. V. Sidorov, and D. B. Stamenov, Eur. Phys. J. C **23**, 479 (2002).
[34] J. Blumlein and H. Bottcher, Nucl. Phys. **B636**, 225 (2002).
[35] Y. Goto *et al.* (Asymmetry Analysis Collaboration), Phys. Rev. D **62**, 034017 (2000); M. Hirai, S. Kumano, and N. Saito (Asymmetry Analysis Collaboration), Phys. Rev. D **69**, 054021 (2004).
[36] E. Leader, A. V. Sidorov, and D. B. Stamenov, Phys. Rev. D **73**, 034023 (2006).
[37] C. Bourrely, J. Soffer, and F. Buccella, Eur. Phys. J. C **23**, 487 (2002).
[38] G. Altarelli, R. D. Ball, S. Forte, and G. Ridolfi, Nucl. Phys. **B496**, 337 (1997); Acta Phys. Pol. B **29**, 1145 (1998); S. Forte, M. Mangano, and G. Ridolfi, Nucl. Phys. **B602**, 585 (2001).
[39] G. Altarelli, R. D. Ball, S. Forte, and G. Ridolfi, Nucl. Phys. **B496**, 337 (1997).
[40] M. Hirai and S. Kumano (Asymmetry Analysis Collaboration), Nucl. Phys. **B813**, 106 (2009).
[41] A. N. Khorramian, A. Mirjalili, and S. A. Tehrani, J. High Energy Phys. 10 (**2004**) 062.
[42] S. Atashbar Tehrani and A. N. Khorramian, J. High Energy Phys. 07 (**2007**) 048.
[43] S. Atashbar Tehrani, A. N. Khorramian, S. T. Monfared, and F. Arbabifar, AIP Conf. Proc. **1374**, 391 (2011).
[44] F. Arbabifar, A. N. Khorramian, S. T. Monfared, and S. A. Tehrani, Int. J. Mod. Phys. A **26**, 625 (2011).
[45] A. N. Khorramian, S. Atashbar Tehrani, F. Olness, S. T. Monfared, and F. Arbabifar, Nucl. Phys. B, Proc. Suppl. **207–208**, 65 (2010).
[46] B. Adeva *et al.* (SMC Collaboration), Phys. Lett. B **420**, 180 (1998).
[47] M. G. Alekseev *et al.* (COMPASS Collaboration), Phys. Lett. B **660**, 458 (2008).
[48] M. G. Alekseev *et al.* (COMPASS Collaboration), Phys. Lett. B **680**, 217 (2009).
[49] E. Leader, A. V. Sidorov, and D. B. Stamenov, Phys. Rev. D **82**, 114018 (2010).
[50] D. de Florian, O. A. Sampayo, and R. Sassot, Phys. Rev. D **57**, 5803 (1998); D. de Florian and R. Sassot, Phys. Rev. D **62**, 094025 (2000); D. de Florian, G. A. Navarro, and R. Sassot, Phys. Rev. D **71**, 094018 (2005).
[51] D. de Florian and R. Sassot, Phys. Rev. D **62**, 094025 (2000).
[52] D. de Florian, G. A. Navarro, and R. Sassot, Phys. Rev. D **71**, 094018 (2005).
[53] D. de Florian, R. Sassot, M. Stratmann, and W. Vogelsang, Phys. Rev. Lett. **101**, 072001 (2008).
[54] D. de Florian, R. Sassot, M. Stratmann, and W. Vogelsang, Phys. Rev. D **80**, 034030 (2009).
[55] M. Soleymaninia, A. N. Khorramian, S. M. Moosavinejad, and F. Arbabifar, Phys. Rev. D **88**, 054019 (2013).
[56] M. G. Alekseev *et al.* (COMPASS Collaboration), Phys. Lett. B **693**, 227 (2010).
[57] M. Arneodo *et al.* (NMC Collaboration), Phys. Lett. B **364**, 107 (1995).
[58] K. Abe *et al.* (SLAC E143 Collaboration), Phys. Lett. B **452**, 194 (1999).
[59] S. D. Bass, Rev. Mod. Phys. **77**, 1257 (2005).
[60] D. Adams *et al.* (SMC Collaboration), Phys. Lett. B **336**, 125 (1994).
[61] K. Abe *et al.* (E154 Collaboration), Phys. Lett. B **404**, 377 (1997).
[62] S. Wandzura and F. Wilczek, Phys. Lett. **72B**, 195 (1977).
[63] D. de Florian, M. Stratmann, and W. Vogelsang, Phys. Rev. D **57**, 5811 (1998).
[64] A. N. Sisakian, O. Y. Shevchenko, and V. N. Samoilov, arXiv:hep-ph/0010298.
[65] E. Leader, A. V. Sidorov, and D. B. Stamenov, arXiv:1212.3204.
[66] M. Hirai, S. Kumano, T.-H. Nagai, and K. Sudoh, Phys. Rev. D **75**, 094009 (2007).
[67] S. Albino, B. A. Kniehl, and G. Kramer, Nucl. Phys. **B803**, 42 (2008).

[68] D. de Florian, R. Sassot, and M. Stratmann, Phys. Rev. D **75**, 114010 (2007); , Phys. Rev. D **76**, 074033 (2007).
[69] A. D. Martin, R. G. Roberts, W. J. Stirling, and R. S. Thorne, Eur. Phys. J. C **28**, 455 (2003).
[70] P. Jimenez-Delgado, A. Accardi, and W. Melnitchouk, arXiv:1310.3734.
[71] J. Soffer, Phys. Rev. Lett. **74**, 1292 (1995).
[72] C. Amsler *et al.* (Particle Data Group), Phys. Lett. B **667**, 1 (2008).
[73] H. J. Lipkin, Phys. Lett. B **214**, 429 (1988); , Phys. Lett. B **230**, 135 (1989); F. E. Close and R. G. Roberts, Phys. Rev. Lett. **60**, 1471 (1988); M. Roos, Phys. Lett. B **246**, 179 (1990); Z. Dziembowski and J. Franklin, J. Phys. G **17**, 213 (1991); P. G. Ratcliffe, Phys. Lett. B **242**, 271 (1990); Phys. Lett. B **365**, 383 (1996); , arXiv:hep-ph/0012133; S. L. Zhu, G. Sacco, and M. J. Ramsey-Musolf, Phys. Rev. D **66**, 034021 (2002); E. Leader and D. B. Stamenov, Phys. Rev. D **67**, 037503 (2003).
[74] M. A. Ahmed and G. G. Ross, Nucl. Phys. **B111**, 441 (1976); G. Altarelli and G. Parisi, *ibid.* **B126**, 298 (1977).
[75] R. Mertig and W. L. van Neerven, Z. Phys. C **70**, 637 (1996); W. Vogelsang, Phys. Rev. D **54**, 2023 (1996); Nucl. Phys. **B475**, 47 (1996).
[76] M. Stratmann and W. Vogelsang, Phys. Rev. D **64**, 114007 (2001).
[77] G. Altarelli, R. K. Ellis, G. Martinelli, and S. Y. Pi, Nucl. Phys. **B160**, 301 (1979).
[78] A. Piccione and G. Ridolfi, Nucl. Phys. **B513**, 301 (1998).
[79] A. Accardi and W. Melnitchouk, Phys. Lett. B **670**, 114 (2008).
[80] S. Moch, J. A. M. Vermaseren, and A. Vogt, Nucl. Phys. **B726**, 317 (2005).
[81] J. Blümlein and A. Tkabladze, Nucl. Phys. B, Proc. Suppl. **79**, 541 (1999).
[82] A. Vogt, Comput. Phys. Commun. **170**, 65 (2005).
[83] F. James and M. Roos, Comput. Phys. Commun. **10**, 343 (1975); Minuit: Function Minimization and Error Analysis, CERN Program Library Long Writeup D506 (1994).
[84] A. D. Martin, W. J. Stirling, R. S. Thorne, and G. Watt, Eur. Phys. J. C **63**, 189 (2009).
[85] J. Pumplin, D. Stump, R. Brock, D. Casey, J. Huston, J. Kalk, H. L. Lai, and W. K. Tung, Phys. Rev. D **65**, 014013 (2001).
[86] E. Leader, A. V. Sidorov, and D. B. Stamenov, Phys. Rev. D **84**, 014002 (2011).
[87] A. Sissakian, O. Shevchenko, and O. Ivanov, Eur. Phys. J. C **65**, 413 (2010).
[88] A. Airapetian *et al.* (HERMES Collaboration), Phys. Rev. Lett. **84**, 2584 (2000).
[89] B. Adeva *et al.* (Spin Muon Collaboration), Phys. Rev. D **70**, 012002 (2004).
[90] M. Stolarski (COMPASS Collaboration), arXiv:0809.1803.
[91] E. S. Ageev *et al.* (COMPASS Collaboration), Phys. Lett. B **633**, 25 (2006).
[92] M. Alekseev *et al.* (COMPASS Collaboration), arXiv:0802.3023.
[93] M. Alekseev *et al.* (COMPASS Collaboration), Phys. Lett. B **660**, 458 (2008).
[94] J. C. Peng, Eur. Phys. J. A **18**, 395 (2003).
[95] J. Soffer, arXiv:1112.0304.
[96] O. Y. Shevchenko, R. R. Akhunzyanov, and V. Y. Lavrentyev, Eur. Phys. J. C **71**, 1713 (2011).
[97] D. de Florian and W. Vogelsang, Phys. Rev. D **81**, 094020 (2010).
[98] D. Boer *et al.*, arXiv:1108.1713.
[99] D. de Florian and Y. R. Habarnau, Eur. Phys. J. C **73**, 2356 (2013).
[100] Program summary: http://particles.ipm.ir/links/QCD.htm.